

Jurassic magmatism and sedimentation in the Palen Mountains, southeastern California: Implications for regional tectonic controls on the Mesozoic continental arc

Benjamin N. Fackler-Adams*
Cathy J. Busby
James M. Mattinson

Department of Geological Sciences, University of California at Santa Barbara,
Santa Barbara, California 93106

ABSTRACT

Stratigraphic and geochronologic data from three regionally extensive Mesozoic stratigraphic units exposed in the Palen Mountains, California, provide constraints on (1) the duration of supermature craton-derived sedimentation within the Jurassic magmatic arc, (2) the timing of cessation of Jurassic magmatism in southeastern California, and (3) plate-margin scale correlation of siliciclastic units that record the initiation of Gulf of Mexico rift-related sedimentation. These three regionally extensive units occur as a 7.5-km-thick conformable succession in the Palen Mountains, consisting dominantly of (1) eolian quartzose sandstone (upper member of the Palen formation), (2) silicic volcanoclastic rocks and associated plugs and domes (Dome Rock sequence), and (3) terrigenous sedimentary rocks (McCoy Mountains Formation).

Our data constrain the age of the eolian quartz arenite (upper Palen formation) to Middle to latest Early Jurassic time (Toarcian to Bathonian) because its upper part is locally interbedded with the basal Dome Rock sequence, which we have dated as 174 ± 8 Ma (U-Pb zircon). This age for the eolian quartz arenite suggests that potentially correlative Middle Jurassic cratonal rocks on the present-day Colorado Plateau include the Page Sandstone, eolian parts of the Carmel Formation, and the Temple Cap Sandstone, all of southwestern Utah and northern Arizona. Correlation with the Navajo Sandstone can not be precluded, although this seems unlikely because one must assume the maximum error on both the U-Pb zircon age and the uncertainties on the stage boundaries to obtain an overlap of only 1 m.y.

Our stratigraphic data also document a locally interfingering contact between the Dome Rock sequence and the overlying McCoy Mountains Formation, the chronostratigraphic extent and tectonic significance of which are controversial. We have dated three units along and below this contact: (1) a green ignimbrite concordantly overlain by (2) a pink ignimbrite capped by a pink nonwelded tuff, and (3) a pink plug-dome complex that intrudes the pink ignimbrite and the dome talus of which interfingers with the pink tuff. The dome talus also interfingers with maroon siltstone, a unit that is regionally typical of the basal McCoy Mountains Formation. The U-Pb zircon dates of the green ignimbrite and the pink ignimbrite overlap within error (155 ± 8 Ma and 162 ± 3 Ma, respectively). U-Pb data for zircon fractions from the plug-dome complex do not further constrain the age of the upper Dome Rock sequence, due to complex inheritance and lead loss, but are consistent with the other dates. Taken together, these data demonstrate that the lowermost McCoy Mountains Formation is late Middle to early Late Jurassic (Bathonian to Oxfordian) in age.

A late Middle to early Late Jurassic age for the lower unit of the McCoy Mountains Formation supports the previous interpretation that development of the extensional-transtensional McCoy basin (southeastern California and western Arizona) and the Bisbee basin (southeastern Arizona) was broadly coeval, within the limits of sparse isotopic data in southeastern Arizona, and was the result of rifting during opening of the Gulf of Mexico. We suggest that the much more abrupt volcanic to sedimentary transition in southeastern California, relative to that recorded in southern Arizona, may reflect a greater component of strike-slip faulting relative to extension in a regionally transtensional regime. We speculate that this resulted from along-strike variation in plate-margin orientation.

INTRODUCTION

Jurassic strata in the Palen Mountains, southeastern California (Fig. 1A), record the local initiation, development, and demise of continental arc magmatism. These volcanic rocks have previously been loosely determined by regional lithostratigraphic correlations as Middle to Late Jurassic in age (Reynolds et al., 1987; 1989; Tosdal et al., 1989). The volcanic rocks are underlain by eolian quartz arenite, and overlain by the thick siliciclastic McCoy Mountains Formation (Figs. 1 and 2). The ages, and therefore tectonic significance, of these regionally extensive units have been controversial. We document contact relations among these units through detailed facies analysis of volcanic, volcanoclastic, and sedimentary rocks. This analysis, together with U-Pb zircon dating of key volcanic units, constrains both the nature and duration of volcanism in this segment of the Jurassic arc and the ages of the underlying and overlying sedimentary strata. The results of this work permit tectonic reconstructions of interactions between the subduction margin of western North America and the rift margin of the Gulf of Mexico–Atlantic realm.

Eolian quartz arenite at the lower part of the Palen Mountains section has been previously correlated with the Lower Jurassic Navajo Sandstone on the basis of composition and stratigraphic position (Marzolf, 1980; LeVeque, 1982; Hamilton, 1987; Tosdal et al., 1989). The unusual association of supermature craton-derived quartz arenites with volcanic and volcanoclastic rocks has long been recognized in the Mesozoic arc of southwestern North America (Miller and Carr, 1978; Bilodeau and Keith, 1979, 1984, 1986; Marzolf, 1980). Wright et al. (1981) reported a U-Pb zircon date of 190–195 Ma from arc volcanic rocks intercalated with eolian quartz arenite in the Baboquivari Mountains of southeastern Arizona. On the basis of this date, Bilodeau and Keith (1986) correlated eolian quartz arenites in several southern Arizona ranges with the Lower

*e-mail: adams@magic.geol.ucsb.edu

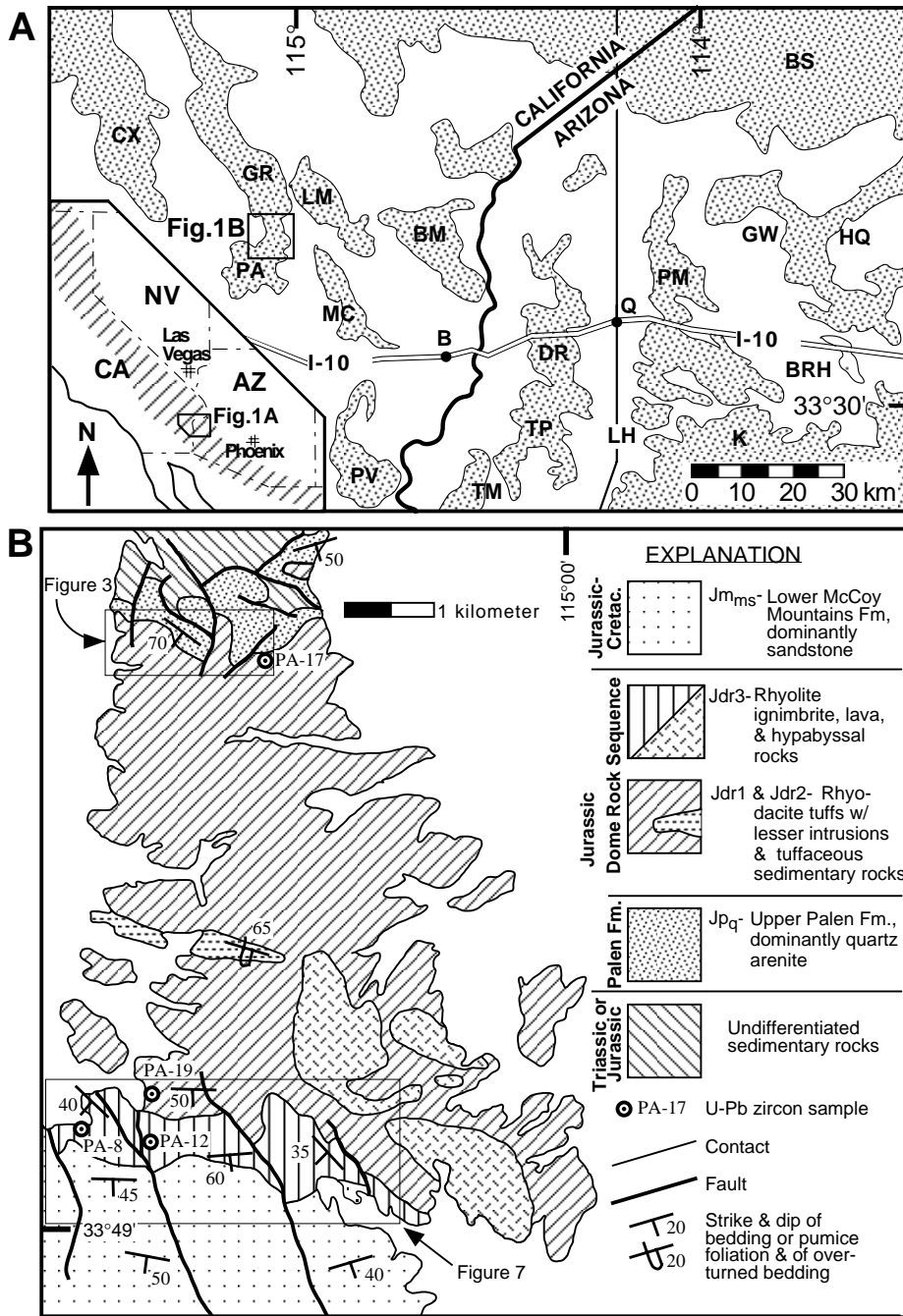


Figure 1. (A) Shaded areas show uplifted Tertiary and older basement. B—Blythe, Q—Quartzsite. Localities referred to in the text include: DR—Dome Rock Mountains, LH—Livingston Hills, MC—McCoy Mountains, PA—Palen Mountains. Other ranges that contain relevant rocks (Palen formation, Dome Rock sequence, McCoy Mountains Formation) include: BM—Big Maria Mountains, BRH—Black Rock Hills, BS—Buckskin Mountains, CX—Coxcomb Mountains, GR—Granite Mountains, GW—Granite wash Mountains, HQ—Harquahala Mountains, K—Kofa Mountains, LM—Little Maria Mountains, PM—Plumosa Mountains, PV—Palo Verde and Mule Mountains, TM—Trigo Mountains, TP—Trigo Peak. Location of map in B is shown by box. The inset shows the location of A and the regional distribution of Jurassic supracrustal arc rocks in southwestern North America (hachured; after Busby-Spera, 1988). (B) Generalized geologic map of the Palen Mountains (after Stone and Pelka, 1989). The map shows the distribution of major rock types and the locations of U-Pb zircon samples (PA-17, PA-19, PA-12, and PA-8). The locations of lithofacies maps in Figures 3 and 7 are shown by boxes.

Jurassic Navajo Sandstone of the Colorado Plateau and its western continuation, the Aztec Sandstone. Because this lithologic association is so unusual, workers have subsequently correlated all supermature quartz arenites interstratified with Jurassic arc volcanic rocks in California and Arizona with the Navajo Sandstone (see references in Busby-Spera et al., 1990a). Recent U-Pb zircon dating of volcanic rocks with interstratified sandstones, however, indicates that deposition of supermature sandstones within the Jurassic arc spanned ~35 m.y. (Riggs et al., 1986, 1993; Busby-Spera, 1988). In this study we documented interfingering relationships between arc

volcanic rocks and eolian quartz arenite and dated the volcanic rocks as late Middle Jurassic using the U-Pb zircon method. These new data further strengthen the hypothesis that the Jurassic arc acted as a depocenter for supermature craton-derived sands throughout much of Jurassic time (Busby-Spera, 1988).

The McCoy Mountains Formation is another poorly understood component in the Mesozoic regional stratigraphic framework of the southwestern Cordillera. It is important because it records the demise of the continental arc and basin development in a tectonic setting whose nature remains controversial. This formation is a

dominantly fluvial siliciclastic unit, as thick as 8 km, exposed in southeastern California and western Arizona (Harding and Coney, 1985; Dickinson et al., 1986, 1987). Until recently, the age and therefore the tectonic setting of the McCoy Mountains Formation have been poorly constrained. Paleomagnetic data were interpreted by Harding et al. (1983) to indicate a pre-Late Jurassic age for the McCoy Mountains Formation. This interpretation was considered invalid for reasons elaborated by Stone et al. (1987) and May (1985); we concur. In addition, fossil angiosperm wood recovered from the upper part of the formation indicate a Late Cretaceous age (Pelka,

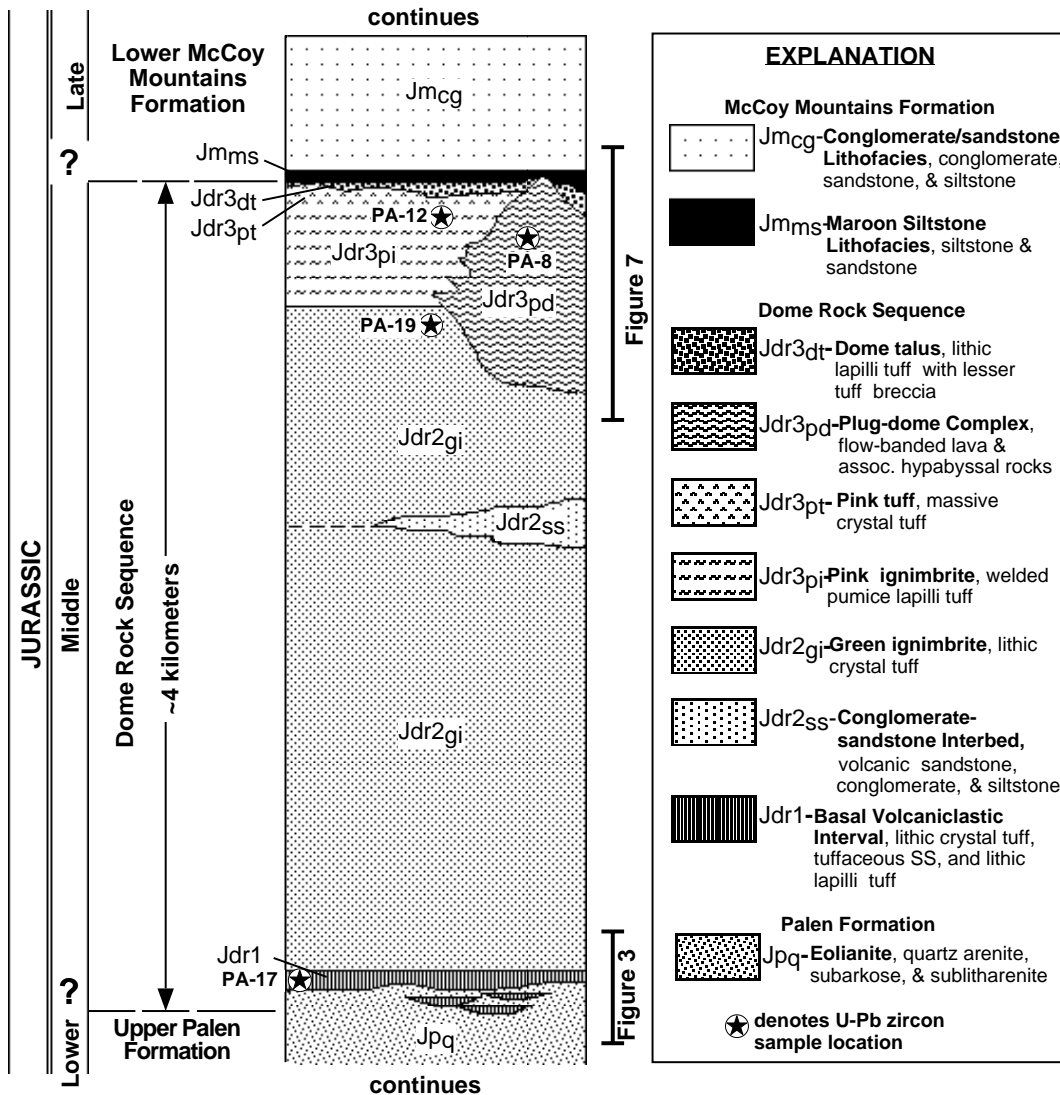


Figure 2. A schematic stratigraphic column of Jurassic rocks in the Palen Mountains, California. The locations of U-Pb zircon samples (PA-17, PA-19, PA-12, and PA-8) are shown by stars. Map units of the Dome Rock sequence are numbered sequentially upward: Jdr1, Jdr2, Jdr3. These units and those below and above (Jpq, Jm_{ms}, and Jm_{cg}) are described in detail in the text and in Table 1. Stratigraphic intervals covered by maps of Figures 3 and 7 are shown by brackets at right of column. The column is approximately to scale.

1973; Stone et al., 1987), and a tuff in the upper part of the formation has yielded a U-Pb zircon crystallization age of 79 ± 2 Ma (Tosdal and Stone, 1994). Prior to our study, no fossil or isotopic ages have been published from the lower part of the McCoy Mountains Formation. The clastic rocks of the upper part of the formation are compositionally distinct from those of the lower part, and in some ranges an angular unconformity locally separates the two parts, suggesting that the lower part may be much older than the Late Cretaceous upper part. For these reasons, the McCoy Mountains Formation has been divided into upper and lower units (Harding and Coney, 1985; Stone and Pelka, 1989; Tosdal and Stone, 1994).

Prior to this study, the only constraints on the maximum age of the lower unit of the McCoy

Mountains Formation were isotopic ages on underlying volcanic rocks of the Dome Rock sequence (Reynolds et al., 1987; Tosdal et al., 1989). Although previous workers reported conformable and locally interbedded contacts between the underlying volcanic rocks and the basal McCoy Mountains Formation (Crowl, 1979; Harding et al., 1980; Harding and Coney, 1985; Tosdal et al., 1989), most contacts have been interpreted as disconformable (Harding and Coney, 1985; Richard et al., 1985; Tosdal and Stone, 1994). This is the first study to document a conformable, interbedded contact between the Dome Rock sequence and the McCoy Mountains Formation. Our U-Pb zircon dates from these volcanic rocks indicate a late Middle to early Late Jurassic age for the basal McCoy Mountains Formation.

Our new constraints on the age of the Dome Rock sequence and lower McCoy Mountains Formation support correlation of McCoy Basin strata with the broadly coeval basal strata of the Bisbee basin in southeastern Arizona (Dickinson et al., 1987; Busby-Spera et al., 1987, 1989, 1990a). Correlation of tectono-sedimentary events between southeastern California and southeastern Arizona has been difficult because of sparse dating of rocks in both the McCoy and Bisbee basin regions and because of very sparse exposures of Jurassic supracrustal rocks between the two regions (Tosdal et al., 1989). Strata in both the McCoy basin and the Bisbee basin (southeastern Arizona) have been interpreted to record exploitation of the thermally weakened Cordilleran arc by Gulf of Mexico-related rifting

in an extensional to transtensional setting (Dickinson et al., 1986, 1987; Busby-Spera et al., 1990b; Saleeby and Busby, 1992).

REGIONAL GEOLOGIC SETTING

The early Mesozoic magmatic arc of California and Arizona formed at a high angle to Paleozoic structural and stratigraphic trends, probably due to tectonic truncation of the continental margin in late Paleozoic time (Burchfiel and Davis, 1972; Stone and Stevens, 1988; Walker, 1988). The arc thus developed across eugeoclinal settings in northern California, miogeoclinal settings in central California, and cratonal settings in southeastern California to southern Arizona and northern Sonora (Busby-Spera et al., 1990a). Lower Mesozoic strata in southeastern California and western Arizona record a transition from Paleozoic and Triassic cratonal sedimentation to Jurassic continental arc magmatism (Tosdal et al., 1989). Strata that record this transition include the Middle (?) Triassic to Middle Jurassic Buckskin and Vampire Formations in western Arizona (Reynolds et al., 1989) and correlative rocks in the Palen Mountains of southeastern California (Stone and Pelka, 1989). The upper part of this section in the Palen Mountains has been informally referred to as the Palen formation (Pelka, 1973; LeVeque, 1982; Reynolds et al., 1987; 1989). The upper member of the Palen formation is predominantly eolian quartz arenite (LeVeque, 1982).

Arc magmatism during Jurassic time generated a thick sequence of volcanic and volcanoclastic rocks represented throughout southwest Arizona and southeast California by the Dome Rock sequence and its correlatives (Crawl, 1979; Pelka, 1973; Richard et al., 1985; Stone and Kelly, 1988; Stone and Pelka, 1989; Reynolds et al., 1987, 1989; Tosdal et al., 1989). The Dome Rock sequence consists dominantly of quartzphyric rhyolitic to dacitic ash-flow tuff, fallout tuff, lava flows, and hypabyssal intrusions. Local volcanogenic sedimentary rocks consist of tuffaceous sandstone, siltstone, and agglomerate derived directly from volcanic rocks. The Dome Rock sequence has heretofore been loosely constrained as Early to Late Jurassic in age by radiometric dates and lithologic correlations (L. T. Silver, quoted in Crawl, 1979; Reynolds et al., 1989; Tosdal et al., 1989). The Planet and Black Rock volcanic rocks of west-central Arizona, included in the Dome Rock sequence by Tosdal et al. (1989), have yielded U-Pb zircon ages of 154 ± 4 Ma and 156 ± 10 Ma, respectively (Reynolds et al., 1987). Prior to our study, the Dome Rock sequence was not dated by reliable means in the Palen Mountains or elsewhere in California, as discussed below.

Arc volcanic rocks of southwest Arizona and southeast California are overlain by largely allu-

vial siliciclastic sedimentary rocks of the McCoy Mountains Formation (Harding and Coney, 1985). The contact between the Dome Rock sequence and McCoy Mountains Formation has been interpreted as marking the Jurassic cessation of arc magmatism in southeastern California and western Arizona (Tosdal et al., 1989). The age of the basal McCoy Mountains Formation has been poorly constrained prior to the present study.

We chose the Palen Mountains for detailed study because the Palen formation, the Dome Rock sequence, and the McCoy Mountains Formation form a continuously exposed, largely homoclinal south-dipping section approximately 7.5 km thick that lacks any obvious unconformities (Harding and Coney, 1985; Stone and Kelly, 1988; Stone and Pelka, 1989; Figs. 1 and 2). Our studies in the Palen Mountains focused on mapping the contact relations in detail and constraining the ages of all three units using U-Pb zircon geochronology.

STRATIGRAPHY OF JURASSIC ROCKS IN THE PALEN MOUNTAINS

In this section, we present details of the lithologic characteristics and facies relationships of the map units we recognize in the Palen Mountains (Fig. 2). The units we mapped are dominantly weakly foliated with local weak transposition, and are metamorphosed to lower greenschist grade. Protolith names are used throughout the discussion for simplicity. Pyroclastic rocks and mixed pyroclastic-epiclastic rocks are named following Schmid (1981), Fisher and Schminke (1984), and Sparks et al. (1973) (see Table 1 for definitions). Ignimbrite refers to welded or nonwelded material composed predominantly of pumice, crystals, and shards (Sparks et al., 1973). Chronostratigraphic correlations are made using the time scale of Gradstein et al. (1994).

Palen Formation

The Palen formation conformably overlies metamorphosed Permian Kaibab Limestone in the Palen Mountains (Stone and Pelka, 1989). It consists of a basal polyolithic conglomerate and subarkose, overlain by quartz arenite and lesser subarkose and sublitharenite (eolianite [Jp_q], Figs. 2 and 3, Table 1; LeVeque, 1982; Stone and Kelly, 1988; Stone and Pelka, 1989). We have recognized local volcanoclastic interbeds within the eolian quartz arenite (Jp_q) (Table 1, Figs. 4 and 5). The quartz arenite locally exhibits grain-flow cross-stratification, and set heights of as much as 10 m, indicative of eolian deposition in dunes (LeVeque, 1982; Table 1). As a consequence of its eolian origin and stratigraphic position above sedimentary strata of probably Triassic age and

below the Jurassic Dome Rock sequence, the quartz arenite of the Palen formation, as well as in the Vampire Formation in western Arizona, have been correlated with the Lower Jurassic Aztec and Navajo Sandstones (Marzolf, 1980; LeVeque, 1982; Hamilton, 1982, 1987; Tosdal et al., 1989). New data, presented below, suggest that the quartz arenite of the Palen formation is more likely to be correlative with Middle Jurassic eolianites of the Colorado Plateau than with the Early Jurassic Navajo Sandstone.

Dome Rock Sequence

The Dome Rock sequence in the Palen Mountains is approximately 4 km thick, is dominated by crystal tuff and pumice lapilli tuff, and contains lesser lithic lapilli tuff and tuff breccia, hypabyssal intrusions, lava flows, and tuffaceous sedimentary rocks (Fig. 2, Table 1; Pelka, 1973; Stone and Kelly, 1988; Stone and Pelka, 1989). Our mapping and facies and petrographic analysis of the Dome Rock sequence in the Palen Mountains have defined three map units (Jdr1, Jdr 2, and Jdr 3), all of which are subdivided (Table 1, Fig. 2).

Basal Volcanoclastic Unit (Jdr1). The lowermost lithostratigraphic unit in the Dome Rock sequence, the basal volcanoclastic unit (Jdr1, Fig. 2, Table 1), is exposed for a strike distance of approximately 2.5 km across the crest of the Palen Mountains (Fig. 3); the best exposures are on the eastern and western flanks of the range. It comprises three facies: a lithic lapilli tuff lithofacies ($Jdr1_{lt}$) that predominates on the eastern flank of the range and tuff lithofacies ($Jdr1_t$) and tuffaceous sandstone lithofacies ($Jdr1_{ss}$) that predominate on the western flank of the range. These lithofacies are named according to the dominant lithology present, although other rock types occur in each (Table 1).

Lapilli Tuff Lithofacies ($Jdr1_{lt}$). This lithofacies is dominated by rhyodacitic lithic lapilli tuff, and contains minor interstratified lithic crystal tuff and lithic tuff (Table 1). The lithic lapilli tuff comprises ~35% phenocrysts and ~34% lithic fragments in an altered (vitric?) matrix. The lithic fragments are dominantly felsitic volcanics with lesser vitric fragments (altered pumice?). Both lithic types have phenocryst populations similar to the crystal component of the matrix. In addition to the primary pyrogenic detritus, the lapilli tuff lithofacies ($Jdr1_{lt}$) contains a significant volume (as much as ~13%) of quartz-rich sedimentary lithic fragments. Sparse rounded monocrystalline quartz grains are also present. The sedimentary lithic fragments and the rounded monocrystalline quartz are interpreted as material mixed with the pyroclastic detritus during its eruption and/or emplacement in the eolian dune environment recorded by the upper Palen formation eolianite (Jp_q).

TABLE 1. LITHOLOGY, FACIES, AND STRATIGRAPHIC RELATIONS FOR JURASSIC ROCKS IN THE PALEN MOUNTAINS, CALIFORNIA

| Chrono-stratigraphy* | Map unit (thickness) [†] | Unit name | Dominant rock types | Relationships to other units | Textural and outcrop characteristics | |
|--------------------------------------------|-----------------------------------|---------------------------------------------|------------------------------------------------------------------------------------------------|------------------------------------------------------------------------------------------------------------------------------------------------------------------------------------------------------------------------------------------------------------------------------|---------------------------------------------------------------------------------------------------------------------------------------------------------------------------------------------------------------------------------------------------|-----------------------------------------------------------------------------------------------------------------------------------------------------------------------------------------------------------------------------------------------------------------------------------------------------------------------------------------------------------------------------------------------------------------------------------------------------------------------------------------|
| JURASSIC | McCoy Mts. Fm. | Jm _{cg} (>130 m) | Sandstone-conglomerate lithofacies | Feldspathic litharenite, lithic arkose, and sublitharenite | Conformably overlies and is locally interbedded w/ Jm _{ms} | Upward-fining sequences of beds 2–10 m thick. Beds are tabular to lenticular. Crossbedding and parallel lamination common. Sequences typically graded from gray quartzite pebble conglomerate through tan, massive to cross-bedded, coarse-grained, locally calcareous, quartz-rich sandstone to maroon sandstone and siltstone |
| | | Jm _{ms} (0–5 m) | Maroon siltstone lithofacies | Feldspathic litharenite and sublitharenite | Conformably overlies and is locally interbedded w/ Jdr3 _{dt} . Conformably underlies and is locally interbedded w/ Jm _{cg} | Thin to medium, tabular beds of maroon siltstone and silty sandstone. Common parallel lamination and lesser ripple and trough cross lamination. Local lenticular beds and cross bedding |
| | Late | Jdr3 _{dt} (0–40 m) | Dome talus | Rhyolitic lithic lapilli tuff with lesser tuff breccia and minor tuff. Monolithologic | Jdr3 _{pd} is in conformable and locally interfingering contact w/ overlying Jm _{ms} . Jdr3 _{pd} conformably overlies Jdr3 _{pt} | Massive, predominantly clast-supported, monolithologic lithic lapilli tuff and lesser tuff breccia. Lithics are identical to Jdr3 _{pd} and are angular to very angular w/ extremely delicate irregular margins. Shards not preserved. Upper ~10 m commonly contain irregular zones of maroon siltstone matrix. Locally interbedded w/ thin–medium, tabular to lenticular beds of maroon siltstone (as in Jm _{ms}). White and very light tan to light pink in outcrop |
| | | ? | Jdr3 _{pd} [#] (?) | Plug-dome complex | Rhyolite lava flows, intrusions, and associated breccia, massive to flow banded | Jdr3 _{pd} is ovoidal by Jdr3 _{pt} and Jdr3 _{dt} . Jdr3 _{pd} forms hypabyssal intrusions into the pink ignimbrite (Jdr3 _{pt}) |
| | Middle | Jdr3 _{pt} (≤10 m) | Pink tuff | Rhyolitic pumice lapilli tuff, densely welded | Gradationally overlies Jdr3 _{pt} . Overlies Jdr3 _{pd} | Massive crystal tuff. Pumice shreds and shards locally preserved, probably nonwelded. White to pale pink in outcrop |
| | | Jdr3 _{pi} [#] (~475 m) | Pink ignimbrite | Rhyolitic crystal tuff | Conformably overlies Jdr2 _{gi} . Grades upward into Jdr3 _{pt} . Is intruded by Jdr3 _{pd} | Welded pumice lapilli tuff w/ distinct pink color. Sintering of shards and pinching of pumice shreds between crystals evident in thin section |
| | Dome Rock sequence | Jdr3 _{gi} [#] (~475 m) | Green ignimbrite | Rhyodacitic lithic crystal tuff | Jdr2 _{gi} conformably overlies Jdr1 _{lt} , Jdr1 _{ss1} , and Jdr1 _t along a locally intruded contact. Jdr2 _{gi} conformably underlies Jdr3 _{pi} | Structureless except for the upper ~10 m, which are thin to medium, tabular bedded w/ parallel lamination and cross-bedding. Relict vitroclastic texture evident but inadequate for demonstrating welding. Approximately 200 m of volcanic sandstone and conglomerate (Jdr2 _{ss}) intercalated at approximately mid-level in the unit. Green to brownish green in outcrop |
| | | Jdr2 _{ss} (~200 m) | Sandstone-conglomerate lens | Volcanic feldspathic litharenite | Jdr2 _{ss} forms a lenticular body, which pinches out to the east, within unit Jdr2 _{gi} | Thin to medium-bedded tabular and lesser lenticular beds of tuffaceous sandstone interbedded with lesser siltstone, mudstone, and conglomerate. Beds exhibit parallel and cross lamination and rare local high-angle cross-bedding. Dark tan to green in outcrop |
| | | Jdr1 _t (0–10 m) | Tuff lithofacies | Rhyodacitic lithic crystal tuff with lesser tuffaceous sandstone and lithic lapilli tuff | Locally concordantly overlies Jdr1 _{ss1} , elsewhere occurs as lenses in top of Jp _q . Concordantly overlain by Jdr2 _{gi} ; Jdr1 _{lt} , Jdr1 _{ss1} , and Jdr1 _t are lateral equivalents | Thin to medium beds with parallel lamination and local high angle and trough cross-stratification. Also occurs as massive to high-angle cross-stratified lenticular beds within Jp _q . Dark to light gray in outcrop |
| | Early | ? | Jdr1 _{ss} (~25 m) | Tuffaceous sandstone lithofacies | Locally concordantly overlies Jp _q , and occurs as lenses in top of Jp _q . Concordantly overlain by Jdr2 _{gi} ; Jdr1 _{lt} , Jdr1 _{ss1} , and Jdr1 _t are lateral equivalents | Common thin to medium lenticular beds w/ parallel cross lamination. Tan to light gray in outcrop |
| Jdr1 _{lt} [#] (~30 m) | | Lapilli tuff lithofacies | Rhyodacitic lithic lapilli tuff with minor interstratified lithic crystal tuff and lithic tuff | Locally concordantly overlies Jp _q , elsewhere its lower contact is intruded. Occurs as lenses in top of Jp _q . Concordantly overlain by Jdr2 _{gi} . Jdr1 _{lt} , Jdr1 _{ss1} , and Jdr1 _t are lateral equivalents | Medium to thick-bedded lithic lapilli tuff w/ lesser thin to medium beds of laminated and locally cross-bedded crystal tuff and lithic lapilli tuff. Vitroclastic texture and pumice shreds locally preserved. Dark gray in outcrop. | |
| Palen fm. | Jp _q (~300–400 m) | Eolianite | Quartz arenite with lesser subarkose and sublitharenite | Jp _q underlies and interingers with Jdr1 _{lt} and Jdr1 _t . Jp _q overlies polymict conglomerate of uncertain age (Triassic or Jurassic; Stone and Kelly, 1989) | Massive to faintly cross-stratified sandstone. Local set heights to ~10 m. Locally contains volcaniclastic lenses of lithic crystal tuff, tuffaceous sandstone, and lesser lithic lapilli tuff. Tan to pinkish tan in outcrop. | |

TABLE 1. (Continued)

| Unit name | Igneous phenocryst and groundmass mineralogy and sedimentary detrital modes [§] | Interpretation |
|------------------------------------|-------------------------------------------------------------------------------------------------------------------------------------------------------------------------------------------------------------------------------------------------------------------------------------------------------------------------------------------------------------------------------------------------------------------------------------------------------------------------------------------------------------------------------------------|-------------------------------------------------------------------------------------------------------------------------------------------------------------------------------------------------------------------------------------------|
| Sandstone-conglomerate lithofacies | Qm 74 F 10 Lt 16, matrix 17%. Q—dominantly monocrystalline, angular quartz w/ lesser rounded monocrystalline quartz; F—predominantly plagioclase (An 12–60); L—3% felsitic volcanics, 10% felsitic hypabyssal intrusives, 40% clastic quartz sericite, 30% orthoquartzite, 12% quartz-mica tectonite. Accessories: Mu, Hb, sparse opaques, Zr, sphene. (n = 5) | Fluvial channel deposits |
| Maroon siltstone lithofacies | Qm 72 F 12 Lt 16, matrix 16%. Q—dominantly angular monocrystalline quartz w/ up to 36% rounded monocrystalline quartz; F—plagioclase/total feldspar ratio averages 0.86; L—average 82% felsitic and vitric volcanic and lesser hypabyssal lithics. Remainder is quartz-mica tectonite, lesser clastic quartz-mica sericite and orthoquartzite. Accessories: Mu, Hb. (n = 9) | Deposition in a fluvial environment. The sedimentary structures and fine grain size may indicate quiet water, overbank deposition |
| Dome talus | Up to 19% broken crystals of plagioclase ($\leq 8\%$) and K-feldspar ($\leq 8\%$) w/ lesser quartz ($\leq 2\%$). Rare rounded quartz and plagioclase clasts. Groundmass is tuff or siltstone altered to epidote + piemontite + chlorite + sericite. (n = 4) | Dome-collapse-generated breccia and block-and-ash flow deposits. Parts of the dome talus with maroon siltstone matrix and/or interbeds record fluvial reworking of pyroclastic detritus shed from dome |
| Plug-dome complex | Extremely sparse phenocrysts of K-feldspar (up to $\sim 2\%$) and sphene (up to $\sim 2\%$) w/ lesser embayed quartz ($< 1\%$), plagioclase ($< 1\%$), and Hb ($< 1\%$) in a devitrified and recrystallized groundmass w/ locally pervasive spherulites. Trace of zircon. K-spar commonly albitized. (n = 2) | Intrusive plug to extrusive and autoclastic lava dome rocks |
| Pink tuff | 32%–50% phenocrysts (ave. 42%). Dominantly plagioclase (21%–35%; ave. 28%), lesser K-feldspar (ave. 6%), and quartz (ave. 3%). Accessories include Hb (ave. 3%), Bt (ave. 1%), opaques (trace–1%), and sphene (trace). Mafic phenocrysts and entire groundmass moderately to highly altered to by epidote + sericite + chlorite \pm piemontite. (n = 5) | Co-ignimbrite ash of the pink ignimbrite (Jdr3 _{pt}); fine-grained pyroclastic flows generated by elutriation of Jdr3 _{pt} . Jdr3 _{pt} and Jdr3 _{pt} are coeval. |
| Pink ignimbrite | Comprises 14%–48% phenocrysts (ave. $\sim 32\%$), $\sim 24\%$ lithics (2%–46%), and $\sim 44\%$ matrix (31%–65%). Phenocrysts dominantly plagioclase (7%–22%), K-feldspar (3%–11%; ave. 6%), quartz (embayed; trace–15%). Accessories include Bt (1%–2.5%), opaques (trace–1.5%), sphene (trace), Hb (trace–2%). Lithics are aphyric to sparsely phryic vitric volcanics (fiamme) w/ rare rounded quartzite pebbles. Partial phenocryst and complete groundmass replacement by epidote, sericite, and chlorite. (n = 10) | Ash-flow tuff. Thick homogeneous nature suggestive of caldera fill. Jdr3 _{pt} and Jdr3 _{pt} are coeval |
| Green ignimbrite | Comprises 37%–68% phenocrysts (ave. 55%), 24%–58% matrix (ave. 39%), and $< 1\%$ to 10% lithics (ave. 4%)? Phenocrysts include quartz (embayed; ave. 14%), plagioclase (ave. 29%), and K-feldspar (ave. 6%) all dominantly as broken crystals. Accessories include Bt (ave 3%), opaques (ave. 3%), Hb (trace), and sphene (trace). Bedded top is crystal-rich (up to 75%). Lithics are felsitic volcanics. Groundmass and phenocrysts moderately to highly altered to sericite + epidote + chlorite + calcite. (n = 6) | Ash-flow tuff. Lack of pumice blocks indicative of high explosivity. Thick homogeneous nature suggestive of caldera fill. Bedded top is surge and (?) fallout deposits. Sandstone lens (Jdr2 _{ss}) suggests two eruptive events |
| Sandstone-conglomerate lens | Qm 33 F 27 Lt 40, matrix 26%. Q—predominantly angular and rounded monocrystalline with no embayed volcanic grains; F—plagioclase/total feldspar ratio 0.80; L—dominantly volcanic clasts with lesser sedimentary, metasedimentary, metamorphic tectonic, and hypabyssal fragments. Groundmass and mafic accessories recrystallized to epidote and sericite with lesser hematite and calcite. Sericite alignment produces strong mineral foliation. (n = 2) | Dominantly volcanogenic material remobilized between eruptive events of unit Jdr2 _{gi} . Possible fluvial deposits |
| Tuff lithofacies | Comprises 30%–70% pyrogenic material. Up to 70% groundmass. Locally contains up to $\sim 23\%$ rounded quartz and clastic quartz-sericite lithics similar to Jpq. Phenocrysts include volcanic quartz (2%–7%), plagioclase (14%–28%, An 25–32), K-feldspar (up to 4%). Plagioclase/total feldspar ratio of 0.88. Up to 7% relict vitric lithics (pumice). Accessories: Bt (up to 1%), opaques (trace), Hb (trace). Groundmass and mafic accessories recrystallized to epidote + sericite + hematite w/ local calcite replacement. (n = 3) | Attributed to predominantly secondary (water and wind) reworking of rhyodacitic pyroclastic detritus |
| Tuffaceous sandstone lithofacies | Qm 25 F 37 Lt 8, matrix 36% Ave. 40% pyrogenic detritus. Q—roughly equal mix of angular, rounded, and euhedral volcanic quartz; F—plagioclase/total feldspar ratio 0.88, plagioclase (An 28–34), angular-subrounded; L—Ave. 62% of lithics are felsic and vitric volcanics. Hypabyssal lithics common. Remaining lithics are dominantly clastic quartz-sericite similar to Jpq. Framework and matrix altered to epidote, sericite, and chlorite. Locally calcitized. (n = 6) | Attributed to both primary (fallout and surge) and secondary (water and wind reworking) deposition of rhyodacitic pyroclastic detritus |
| Lapilli tuff lithofacies | Comprises 35% phenocrysts, 34% lithics, 31% matrix. Remainder is highly altered groundmass. Phenocrysts include angular and broken quartz (8%), plagioclase (16%, An 30) K-feldspar (6%), and traces of opaques, Bt, and Hb. Lithic fragments $\sim 60\%$ (felsitic \gg vitric $>$ hypabyssal) and $\sim 40\%$ clastic quartz sericite. Whole moderately to highly altered to epidote + sericite + chlorite \pm calcite. (n = 1) | Dominantly deposits of small block-and-ash flows with lesser fall-out, surge, and/or fluvial deposits |
| Eolianite | Qm 88 F 7 Lt 5, matrix 7%. Q—rounded to sub-rounded monocrystalline and polycrystalline, quartz locally highly polygonized and/or replaced by calcite; F—plagioclase/total feldspar ratio 0.83; L—predominantly felsitic volcanics w/ rare quartz-mica tectonite. Matrix is sericite \pm calcite. (n = 3) | Eolian dune deposits. Supermature quartz sands variably contaminated by silicic tuff and volcanoclastic detritus |

*As constrained by this study.

[†]Thickness measured by Jacob's staff or as reported in Stone and Kelly (1988), and Stone and Pelka (1989).[§]See Table 2 for sedimentary petrographic data. Petrographic parameters (Qm, F, and Lt) as defined by Dickinson and Suczek (1979). Modal data based on point counts of 500 or 600 points per thin section.[#]Indicates unit was sampled for U-Pb zircon dating (see Figure 2 and Table 3).

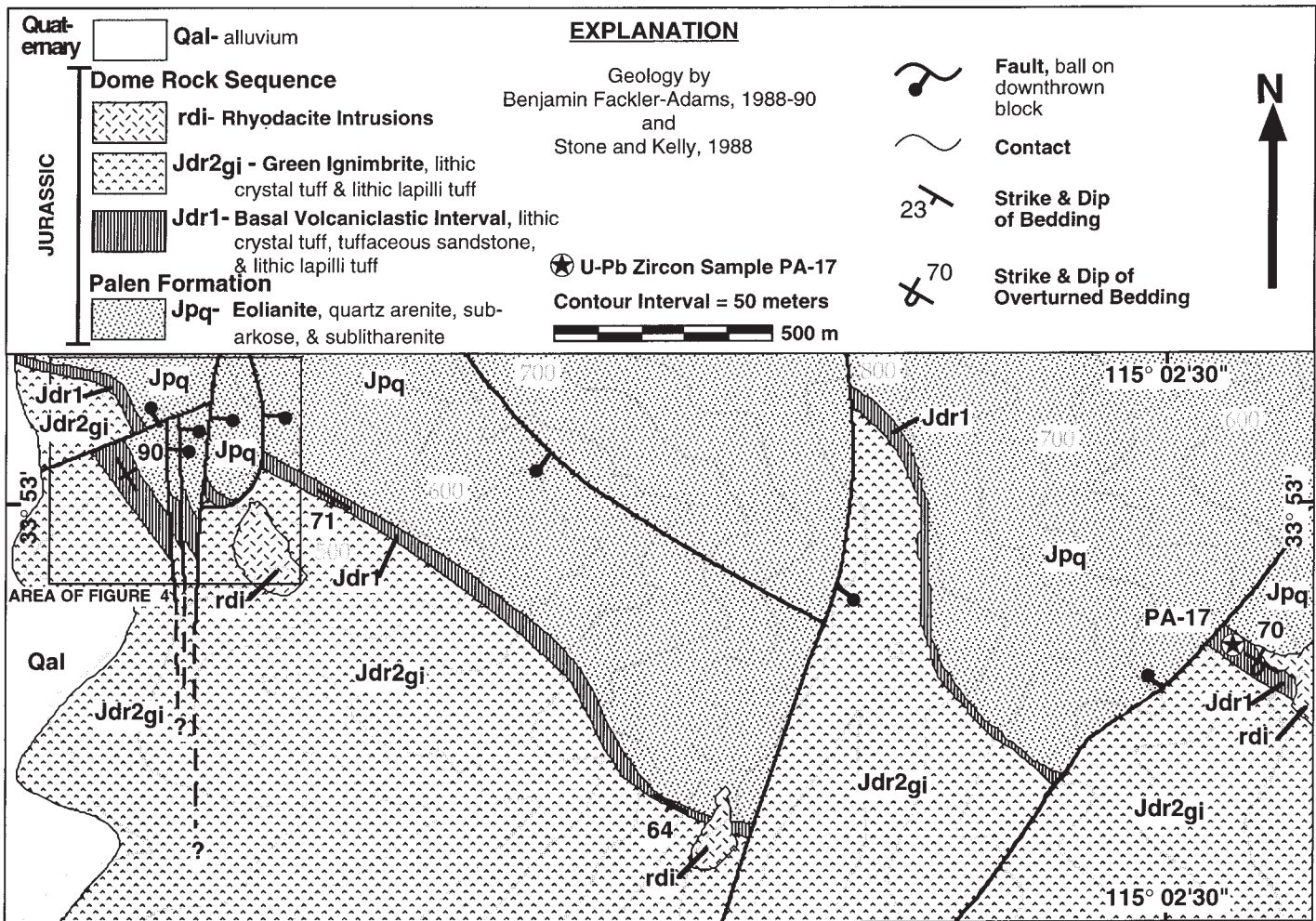


Figure 3. Geologic map of the contact between the upper eolian quartz arenite (Jp_q) of the Triassic-Jurassic Palen formation and the basal volcanoclastic interval ($Jdr1$) of the Jurassic Dome Rock sequence (see location in Fig. 1). Stratigraphic top is toward the south-southwest. The location of U-Pb zircon sample PA-17 is shown by the star. The area of Figure 4 is enclosed by the box on the left. The topography is shown in gray.

On the eastern flank of the range, the lapilli tuff lithofacies ($Jdr1_{it}$) is 30 m thick. It consists of structureless, medium to thick beds of lithic lapilli tuff with lesser thin to medium interbeds of laminated and locally cross-bedded crystal tuff and lithic lapilli tuff. This succession is interpreted as small-volume block and ash flow deposits separated by lesser fallout, surge, and/or fluvial deposits. In this area, the lapilli tuff lithofacies ($Jdr1_{it}$) concordantly and sharply overlies the eolianite (Jp_q) and is concordantly and sharply overlain by the green ignimbrite ($Jdr2_{gi}$), although these contacts are locally intruded by rhyodacite (Fig. 3).

On the western flank of the range, the lapilli tuff lithofacies ($Jdr1_{it}$) is more fine grained and has a higher proportion of lithic crystal tuff than on the eastern flank. It occurs as thin- to medium-bedded lenses and as tabular thin-bedded horizons within larger lenses of the tuff lithofacies ($Jdr1_t$),

all interstratified with the upper part of the eolianite (Fig. 5). The thinner bedding and better stratification of the lapilli tuff lithofacies ($Jdr1_{it}$) on the west flank of the range relative to the east flank suggests at least partial fluvial reworking. For this reason, we sampled this lithofacies for U-Pb zircon dating on the eastern flank of the range.

Tuff Lithofacies ($Jdr1_t$). The tuff lithofacies ($Jdr1_t$) is dominated by rhyodacitic lithic crystal tuff and contains lesser tuffaceous sandstone and lithic lapilli tuff (Table 1). The lithic crystal tuff has 16%–40% phenocrysts, as much as 7% vitric lithic fragments, and as much as 70% altered vitric matrix. It also commonly contains a few percent rounded monocrystalline quartz grains and quartz-rich sedimentary lithic fragments (quartz-sericite clasts; Tables 1 and 2). The tuff occurs as tabular and locally lenticular thin to medium beds with parallel lamination and sparse high-angle and trough cross lamination

(Table 1). The relative importance of primary (fallout and surge) vs. secondary (water and wind reworking) processes in the deposition of these tuffs is unclear.

The tuff lithofacies ($Jdr1_t$) occurs on the western flank of the range where it occurs as lenses within the upper part of the eolianite, and also as a tabular 9-m-thick interval above a 23-m-thick interval of tuffaceous sandstone lithofacies ($Jdr1_{ss}$, Figs. 4 and 5).

Tuffaceous Sandstone Lithofacies ($Jdr1_{ss}$). The tuffaceous sandstone lithofacies ($Jdr1_{ss}$) is dominated by tuffaceous sandstone and contains lesser lithic crystal tuff and minor lithic lapilli tuff (Table 1). The tuffaceous sandstones form a continuum with the tuffs (described above) in terms of their composition, textures, and sedimentary structures, but they are in general more cross-laminated, show more rounding of grains and more variation in rock fragment types, and have

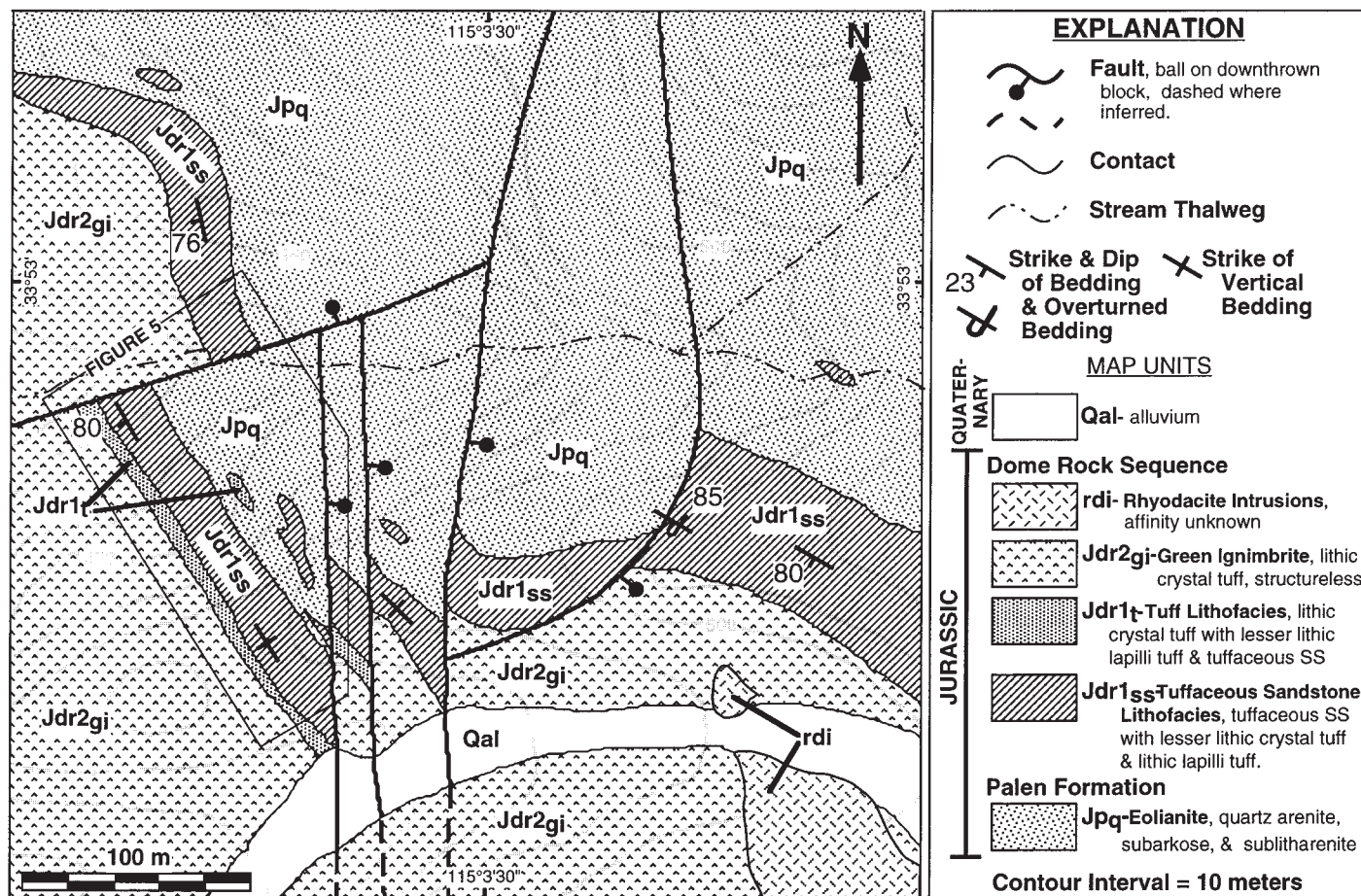


Figure 4. A map of relationships among the upper eolian quartz arenite (Jp_q) of the Triassic-Jurassic Palen formation and map units of the Jurassic Dome Rock sequence, including the tuff and tuffaceous sandstone lithofacies of the basal volcanoclastic interval ($Jdr1_t$ and $Jdr1_{ss}$) and the basal portion of the green ignimbrite ($Jdr2_{gi}$) (see location in Fig. 3). Stratigraphic top is toward the south-southwest. The sequence comprises a conformable succession from the Palen formation (Jp_q) into the lower portion of the Dome Rock sequence ($Jdr2_{gi}$). Note the lenses of volcanoclastic rock within the top of the Palen formation (Jp_q). The area of Figure 5 is enclosed by the box on the left. The topography is shown in gray.

a higher percentage of rounded monocrystalline quartz (Table 1). These characteristics suggest reworking by fluvial processes. The rocks plot in the lithic arkose and feldspathic litharenite compositional fields of Folk (1972; Table 2; Fig. 6).

The lapilli tuffs of the tuffaceous sandstone lithofacies ($Jdr1_{ss}$) have less pyroclastic matrix than the lapilli tuffs of the lapilli tuff lithofacies ($Jdr1_t$), and are better stratified, again suggesting reworking by fluvial processes.

The tuffaceous sandstone lithofacies ($Jdr1_{ss}$) occurs on the western flank of the range as lenses within the upper part of the eolianite (Jp_q) and as a tabular unit conformably overlying the eolianite (Jp_q).

In summary, evidence supporting an inter-fingering contact between the Palen formation and the Dome Rock sequence is both stratigraphic and petrologic, including: (1) intercalation of all three lithofacies of the basal volcanoclastic unit ($Jdr1$) of the Dome Rock sequence with the upper part of the eolian quartz arenite of

the upper Palen formation, and (2) the admixture of significant proportions of rounded monocrystalline quartz grains and quartz arenite clasts with pyroclastic material in both the primary ($Jdr1_t$ and $Jdr1_{ss}$) and secondary lithofacies ($Jdr1_{ss}$) of the basal volcanoclastic unit ($Jdr1$). Therefore, our U-Pb zircon date from the lapilli tuff lithofacies ($Jdr1_t$) (sample PA-17; Figs. 1, 2, and 3; discussed in the following) constrains the age of the eolianite of the upper Palen formation.

Middle Rhyodacite Unit ($Jdr2$). The second major lithostratigraphic unit of the Dome Rock sequence in the Palen Mountains is a green ignimbrite ($Jdr2_{gi}$) that consists of an approximately 3.5-km-thick structureless lithic quartz- and sanidine-phyric rhyodacite tuff. This ignimbrite was previously interpreted as a hypabyssal intrusion (Pelka, 1973). The green ignimbrite ($Jdr2_{gi}$) contains an approximately 200-m-thick lens of sandstone and lesser conglomerate and siltstone ($Jdr2_{ss}$) approximately 2 km from its base (Fig. 2, Tables 1 and 2).

Green Ignimbrite ($Jdr2_{gi}$). The abundance of broken crystals in the green ignimbrite ($Jdr2_{gi}$) indicates a pyroclastic origin, and although vitroclastic texture is evident in thin section, it is inadequately preserved to demonstrate welding. The uppermost 10 m of the green ignimbrite ($Jdr2_{gi}$) consists of tabular-bedded and parallel-laminated tuff and minor lapilli tuff interpreted as fallout deposits. On the basis of its thickness and homogeneity, the green ignimbrite may be interpreted as a caldera-fill deposit, but no caldera margins are preserved within the range or recognized elsewhere. The green ignimbrite ($Jdr2_{gi}$) was sampled approximately 200 m below its top for U-Pb zircon dating (sample PA-19; Table 3; Figs. 1, 2, and 7).

Sandstone-Conglomerate Lens ($Jdr2_{ss}$). The sandstones of the sandstone-conglomerate lens ($Jdr2_{ss}$) are volcanic feldspathic litharenite and plot in the same field as the tuffaceous sandstones of the basal volcanoclastic unit ($Jdr1$, Fig. 6). Sedimentary structures (Table 1) suggest that the

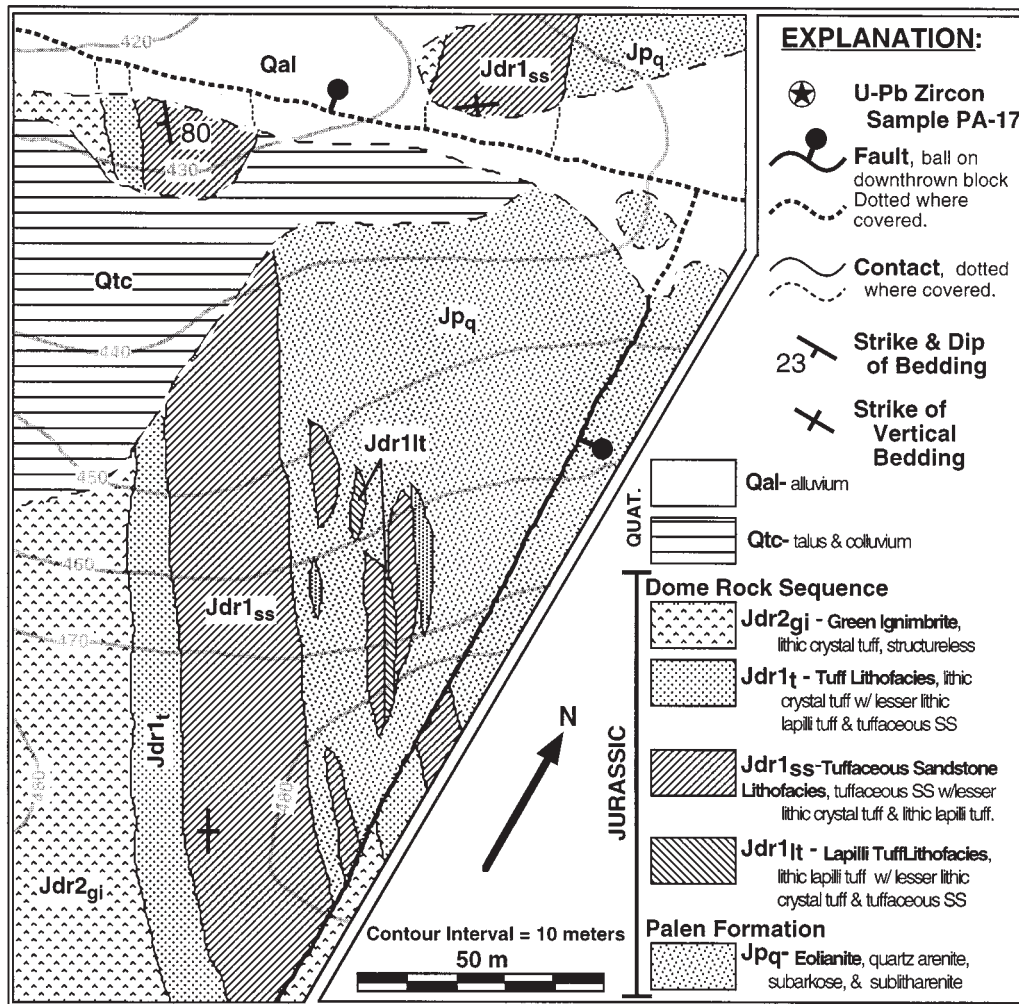


Figure 5. A pace and brunton map of the critical interbedded relationships among the quartz arenites of the Palen formation (Jp_q), and the tuff (Jdr1_t), tuffaceous sandstone (Jdr1_{ss}), and lapilli tuff (Jdr1_{lt}) lithofacies of the basal volcanoclastic interval. Stratigraphic top is toward the west-southwest, and the strata dip vertically to nearly vertically. Concurrent deposition of the eolian quartz-rich sands of the upper Palen formation and the volcanoclastic detritus of the basal Dome Rock sequence is indicated by the lenticular intercalations of tuff, tuffaceous sandstone, and lapilli tuff lithofacies within the upper Palen formation (Jp_q). The topography is shown by gray contours.

sandstone-conglomerate lithofacies is fluvial in origin as well. This fluvial lens indicates a hiatus in the eruption of the green ignimbrite (Jdr2_{gi}), although it may have been extremely brief.

Upper Rhyolite Unit (Jdr3). The third and uppermost major map unit of the Dome Rock sequence in the Palen Mountains is an approximately 500-m-thick interval of pink to white rhyolitic ignimbrite, tuffs, lava flows, and hypabyssal intrusions (Figs. 1B, 7, and 8). The pale color of this interval contrasts markedly with the green ignimbrite below. Associated pink rhyolitic hypabyssal intrusions are also abundant in the upper third of the green ignimbrite. The upper rhyolitic unit is subdivided into four map units.

Pink Ignimbrite (Jdr3_{pi}) and Pink Tuff (Jdr3_{pt}). Approximately 475 m of densely welded pumice lapilli rhyolite tuff (pink ignimbrite [Jdr3_{pi}])

overlies the green ignimbrite (Jdr2_{gi}). Eutaxitic texture in the pink ignimbrite (Jdr3_{pi}) extends to within a few meters of the unit's base, and is parallel to bedding and lamination in the top 10 m of underlying green ignimbrite (Jdr2_{gi}), indicating a conformable contact between the two units. The pink ignimbrite (Jdr3_{pi}) grades upward, over 2–5 m of section, into a structureless to very faintly parallel-stratified crystal tuff, as much as 10 m thick (pink tuff; Jdr3_{pt}), that we interpret as co-ignimbrite ash to the pink ignimbrite (Figs. 2, 7, and 8). The pink ignimbrite (Jdr3_{pi}) exhibits welding textures in hand sample and in thin section (Table 1), whereas the pink tuff (Jdr3_{pt}) shows no evidence of welding.

The thickness and homogeneity of the pink ignimbrite (Jdr3_{pi}) suggest that it represents an intracaldera accumulation, but, as with the green

ignimbrite (Jdr2_{gi}), there are no caldera margins preserved within the range or recognized elsewhere. The pink ignimbrite (Jdr3_{pi}) was sampled for U-Pb zircon dating (sample PA-12; Table 3; Figs. 1, 2, and 7).

Plug-Dome Complex (Jdr3_{pd}). The plug-dome complex (Jdr3_{pd}) consists of aphyric to very sparsely phyric massive to flow-banded rhyolite and minor associated breccia, which we interpret to represent intrusive plug to extrusive and auto-clastic dome rocks (Fig. 8, Table 1). This rhyolite locally intrudes the pink ignimbrite (Jdr3_{pi}), and the pink tuff (Jdr3_{pt}) locally overlies the plug-dome complex (Jdr3_{pd}; Figs. 2, 7, and 8). Therefore, the pink ignimbrite (Jdr3_{pi}) and the pink tuff (Jdr3_{pt}), which record the same eruption (Table 1), are contemporaneous with the plug-dome complex (Jdr3_{pd}). We sampled the plug-

dome complex (Jdr3_{pd}) for U-Pb zircon dating (sample PA-8; Table 3; Figs. 1, 2, and 7).

Dome Talus (Jdr3_{dt}). The dome talus (Jdr3_{dt}) consists mostly of lithic lapilli tuff that is dominantly clast supported and monolithologic, and lesser tuff breccia and minor tuff. The lithic fragments are crystal-poor rhyolite identical to the plug-dome complex rhyolite. The interstitial matrix is highly altered but appears similar in composition to the lithic fragments, except that it is slightly enriched in crystals that are broken. The lithic fragments range from angular to very angular; common extremely delicate, irregular margins indicate little or no postemplacement reworking. These rocks are compositionally and texturally like modern dome-collapse-generated breccias and block and ash flow deposits, such as those at Mount Unzen (Nakada and Fujii, 1993; Yamamoto et al., 1993), Mount St. Helens (Mellors et al., 1988), and Volcán de Colima (Rodríguez-Elizarrarás et al., 1991). We interpret them as block-and-ash flow deposits and talus shed from a dome or domes represented by the plug-dome complex (Jdr3_{pd}; Figs. 7 and 8).

The upper part of the dome talus (Jdr3_{dt}) locally contains maroon siltstone interbeds, or consists of massive monolithic rhyolite breccia with a maroon siltstone or sandstone matrix (Fig. 8). The maroon siltstone-sandstone interbeds are thin to medium tabular beds with parallel laminations and local cross lamination. The compositional and textural characteristics of the maroon siltstone-sandstone interbeds are identical to those of the maroon siltstone lithofacies of the lower McCoy Mountains Formation (Jm_{ms}, Fig. 9, Tables 1 and 2). The breccia with maroon siltstone and sandstone matrix occurs as lenses as thick as 30 cm within the lithic lapilli tuff of the dome talus (Jdr3_{dt}) and as an overlying interval as thick as 12 m (column C, Fig. 8). We interpret those parts of the dome talus (Jdr3_{dt}) containing maroon siltstone-sandstone to record fluvial reworking and addition of nonpyrogenic fluvial sediment to the primary pyroclastic detritus of the dome talus (Jdr3_{dt}, Fig. 9). The upper part of the dome talus (Jdr3_{dt}) thus records increased reworking of primary volcanic products by fluvial processes and gradual introduction of nonpyrogenic detritus typical of the McCoy Mountains Formation.

In summary, the upper rhyolitic unit (Jdr3) consists of a basal pink ignimbrite (Jdr3_{pi}) that has a conformable basal contact, gradationally overlain by a co-ignimbrite ash deposit (pink tuff; Jdr3_{pt}). The pink ignimbrite (Jdr3_{pi}) and underlying strata are intruded by rhyolites of the plug-dome complex (Jdr3_{pd}), whereas the co-ignimbrite ashes were locally deposited upon its eruptive products. These field relations indicate that eruption of all of the rhyolites occurred coevally and immediately followed eruption of

the green ignimbrite (Jdr2_{gi}). Dates from the upper rhyolite unit (Jdr3) and the green ignimbrite (discussed below) support this interpretation. Furthermore, interstratification of maroon siltstone typical of the basal McCoy Mountains Formation with primary eruptive products of the upper rhyolite unit (Jdr3) indicates that these units are in part coeval.

McCoy Mountains Formation

The McCoy Mountains Formation in the Palen Mountains is an approximately 5-km-thick section of sandstone, conglomerate, siltstone, and mudstone. It concordantly overlies the Dome Rock sequence and its top is faulted against rocks inferred to belong to the Dome Rock sequence, or against members of the lower McCoy Mountains Formation (Stone and Pelka, 1989). As discussed above, the lower McCoy Mountains Formation is compositionally distinct from the upper McCoy Mountains Formation, and prior to this study, it has been poorly constrained to between Early or Middle Jurassic and Late Cretaceous time.

Lower McCoy Mountains Formation (Jm). Our observations of the McCoy Mountains Formation in the Palen Mountains were limited to the lowermost ~130 m of the lower McCoy Mountains Formation, which consists of a maroon siltstone lithofacies (Jm_{ms}) and an overlying sandstone-conglomerate lithofacies (Jm_{cg}; Figs. 7 and 8). Lithofacies are named according to the dominant lithology although maroon siltstone, sandstone, and conglomerate all occur in both the maroon siltstone lithofacies (Jm_{ms}) and the sandstone-conglomerate lithofacies (Jm_{cg}). These lithofacies together correspond to “basal sandstone member 1” of Harding and Coney (1985), but we have subdivided it into two lithofacies because they form mappable units (Fig. 7) and because rocks identical to these lithofacies occur within the underlying Dome Rock sequence. In addition, the maroon siltstone lithofacies may be regionally extensive because maroon siltstone also is present at the base of the McCoy Mountains Formation in the Dome Rock Mountains and Livingston Hills of western Arizona (Tosdal and Stone, 1994; Fig. 1).

Maroon Siltstone Lithofacies (Jm_{ms}). The lowermost unit of the McCoy Mountains Formation in the Palen Mountains, the maroon siltstone lithofacies (Jm_{ms}), is a laterally discontinuous mappable horizon (~0–10 m thick) between the dome talus (Jdr3_{dt}) at the top of Dome Rock sequence and the sandstone-conglomerate lithofacies (Jm_{cg}) of the McCoy Mountains Formation (Fig. 8). Siltstone and sandstone of the maroon siltstone lithofacies (Jm_{ms}) and interbeds in the dome talus (Jdr3_{dt}) are sublitharenite, feldspathic litharenite, and subarkose (Fig. 9). Maroon siltstones and sandstones of this litho-

facies are identical to the maroon siltstone and sandstone interbeds within the upper part of the dome talus (Jdr3_{dt}) (Fig. 9, Table 2). These compositions in part corroborate the quartz-rich nature of “basal sandstone member 1” reported elsewhere (Table 2, columns PB1, MB1, and DB1; data from Harding and Coney [1985]). However, the high variability in composition of siltstone and sandstone in both units (Jm_{ms} and Jdr3_{dt}) reflects contamination of the quartz-rich siliciclastic sediment with varying amounts of pyroclastic detritus from the dome talus (Jdr3_{dt}). The maroon siltstone lithofacies (Jm_{ms}) contains common parallel lamination and lesser ripple and trough cross lamination, and is predominantly fine grained, indicating deposition in a fluvial overbank environment. These deposits are identical to the maroon siltstone and sandstone interbeds in the dome talus (Jdr3_{dt}). The maroon siltstone lithofacies also contains buff, locally calcareous sandstone and granule conglomerate beds thinner than, but similar to, those of the overlying sandstone-conglomerate lithofacies (Jm_{cg}), indicating an interfingering contact.

Sandstone-Conglomerate Lithofacies (Jm_{cg}). The sandstone-conglomerate lithofacies (Jm_{cg}) overlies the maroon siltstone lithofacies and, locally, the dome talus (Jdr3_{dt}) (Fig. 8). The sandstone-conglomerate lithofacies (Jm_{cg}) consists predominantly of erosionally based, upward-fining sequences, 2–10 m thick, of tabular to lenticular beds with common cross lamination and planar lamination. These sequences typically grade from gray quartzite pebble- to granule-conglomerate, through tan, massive to cross-bedded, coarse-grained, locally calcareous quartz-rich sandstone, to maroon sandstone and siltstone. We agree with the interpretation of Harding and Coney (1985) that these rocks represent the deposits of channels in a fluvial system. Sandstone of the sandstone-conglomerate lithofacies (Jm_{cg}) is feldspathic litharenite, sublitharenite, and lithic arkose (Fig. 9). These compositions are more lithic rich than reported by Harding and Coney (1985) for “basal sandstone member 1” (see comparison in Table 2), but their samples may have come from higher in the unit than ours.

U-PB ZIRCON GEOCHRONOLOGY

The U-Pb zircon isotopic dating method was chosen for this study because regional and contact metamorphism, and concomitant alkali-element exchange have rendered these volcanic rocks unsuitable for dating by the K/Ar, ⁴⁰Ar/³⁹Ar, or Rb/Sr methods. For example, one sample of the green ignimbrite (Jdr2_{gi}) yielded a K/Ar biotite age of 69 ± 2 Ma (Stone and Kelley, 1988), probably reflecting a thermal or fluid-migration event related to emplacement of a

TABLE 2. PETROGRAPHIC DATA FOR JURASSIC SEDIMENTARY ROCKS IN THE PALEN MOUNTAINS, CALIFORNIA

| Map unit Sample number | Jp _q | | | Jdr _{1ss} | | | | | | Jdr _{2ss} | | Interbeds in Jdr _{3dt} | | |
|-------------------------------------------|-----------------|-------|-------|--------------------|-------|-------|-------|-------|--------|--------------------|-------|---------------------------------|-------|-------|
| | PA-14 | PA-18 | PA-78 | PA-33D | PA-35 | PA-71 | PA-73 | PA-75 | PA-76A | PA-7 | PA-11 | PA-23 | PA-24 | PA-28 |
| Petrographic Modes (%)[†] | | | | | | | | | | | | | | |
| Monocrystalline rounded Q | 85.2 | 77.2 | 75.4 | 10.3 | 5.4 | 7.3 | 10.6 | 2.0 | 3.3 | 3.3 | 4.1 | 28.4 | 36.3 | 18.4 |
| Monocrystalline angular Q | 0 | 0 | 0 | 7.4 | 6.6 | 6.2 | 4.4 | 3.4 | 6.3 | 18.2 | 22.2 | 22.0 | 25.5 | 34.5 |
| Volcanic Q (embayed) | 0 | 0 | 0 | 4.1 | 2.2 | 3.2 | 1.7 | 1.6 | 3.4 | 0.0 | 0.0 | 0.6 | 0.8 | 1.7 |
| P | 2.7 | 3.9 | 9.8 | 23.8 | 28.4 | 17.8 | 13.8 | 14.1 | 19.5 | 13.5 | 17.5 | 11.2 | 8.2 | 6.2 |
| K | 0.1 | 2.2 | 1.4 | 2.8 | 4.2 | 0 | 2.4 | 3.3 | 3.2 | 3.8 | 4.1 | 1.6 | 2.4 | 2.0 |
| A | 0.5 | 0.0 | 1.6 | 3.2 | 3.0 | 1.4 | 3.2 | 4.0 | 2.5 | 1.2 | 0.7 | 2.2 | 3.2 | 2.8 |
| Monocrystalline l | 0.4 | 0.0 | 2.6 | 1.3 | <1 | 2.2 | 1.4 | 1.1 | 1.7 | 0.5 | 1.1 | 1.0 | 0.4 | 1.2 |
| L—volcanic [§] | 0 | 10.0 | 6.0 | 12.8 | 19.2 | 15.3 | 19.2 | 10.3 | 17.1 | 20.0 | 17.3 | 11.8 | 4.4 | 9.2 |
| L—sedimentary [#] | 0 | 0 | 0 | 2.7 | 4.1 | 3.3 | 3.1 | 3.1 | 4.5 | 6.8 | 5.4 | 0 | 0 | 0 |
| L—tectonites | 0 | 0 | 0 | 0 | 0 | 0 | 0 | 0 | 0 | 0.2 | 0.8 | 1.5 | 0.0 | 1.2 |
| L—hypabyssal | 0 | 0 | 0 | 0.2 | 2.1 | 5.1 | 0.3 | 1.3 | 0.2 | 1.8 | 1.0 | 0 | 0 | 0 |
| L—l | 0.4 | 0 | 0 | 0.5 | 2.3 | 1.9 | 1.9 | 3.4 | 1.1 | 1.8 | 2.3 | 0.5 | 2.1 | 0.6 |
| L—total | 0.4 | 10.0 | 6.0 | 16.2 | 27.7 | 25.6 | 24.5 | 18.1 | 22.9 | 30.6 | 26.8 | 13.8 | 6.5 | 11.0 |
| % Interstitial Material | 10.7 | 6.7 | 3.2 | 30.8 | 22.5 | 36.3 | 38.0 | 52.4 | 37.2 | 28.8 | 23.5 | 19.2 | 16.6 | 22.2 |
| Total | 100.0 | 100.0 | 100.0 | 99.9 | 100.0 | 100.0 | 100.0 | 100.0 | 100.0 | 99.9 | 100.0 | 100.0 | 99.9 | 100.0 |
| P/Total Feldspar | 1.0 | 0.6 | 0.9 | 0.9 | 0.9 | 1.0 | 0.9 | 0.8 | 0.9 | 0.8 | 0.8 | 0.9 | 0.8 | 0.8 |
| P (%Anorthite) | N.D. | N.D. | N.D. | 28 | 34 | 30 | 32 | 25 | 31 | 37 | 33 | N.D. | N.D. | N.D. |
| Qm F Lt Modes (%) | | | | | | | | | | | | | | |
| Q monocrystalline | 96.4 | 82.7 | 81.4 | 33.7 | 19.1 | 27.8 | 29.1 | 16.5 | 22.2 | 31.0 | 35.2 | 65.7 | 78.5 | 74.0 |
| Feldspar | 3.2 | 6.5 | 12.1 | 41.2 | 43.8 | 29.6 | 28.2 | 40.9 | 38.7 | 24.9 | 28.9 | 16.5 | 13.3 | 11.1 |
| L—total | 0.5 | 10.7 | 6.5 | 25.1 | 37.2 | 42.6 | 42.7 | 42.6 | 39.1 | 44.1 | 35.9 | 17.8 | 8.2 | 14.9 |
| L—(% by type) | | | | | | | | | | | | | | |
| V—felsitic | 0 | 100.0 | 97.0 | 50.3 | 44.8 | 59.8 | 49.1 | 52.1 | 68.4 | 23.0 | 16.1 | 78.0 | 72.3 | 79.6 |
| V—microlitic | 0 | 0 | 0 | 0 | 0 | 0 | 0 | 0 | 0 | 13.1 | 17.1 | 0 | 0 | 0 |
| V—lathwork | 0 | 0 | 0 | 0 | 0 | 0 | 0 | 0 | 0 | 29.5 | 27.8 | 0 | 0 | 0 |
| V—vitric | 0 | 0 | 0 | 28.2 | 24.6 | 0.0 | 29.3 | 4.8 | 5.9 | 0 | 0 | 3.4 | 7.4 | 4.0 |
| V—hypabyssal | 0 | 0 | 0 | 2.5 | 7.6 | 19.9 | 1.2 | 7.2 | 1.3 | 5.9 | 10.2 | 0 | 0 | 0 |
| Clastic —Q sericite | 0 | 0 | 0 | 16.6 | 14.8 | 12.9 | 12.7 | 17.1 | 19.6 | 11.1 | 10.7 | 0 | 0 | 0 |
| Orthoquartzite | 0 | 0 | 0 | 0 | 0 | 0 | 0 | 0 | 0 | 11.3 | 12.1 | 0 | 0 | 0 |
| Tectonite | 0 | 0 | 3 | 0 | 0 | 0 | 0 | 0 | 0 | 0.3 | 1.2 | 15.1 | 4.4 | 10.9 |
| L—l | 0 | 0 | 0 | 2.5 | 8.3 | 7.4 | 7.8 | 18.8 | 4.8 | 5.8 | 4.7 | 3.4 | 15.9 | 5.5 |
| QpLsLv Modes (%) | | | | | | | | | | | | | | |
| Q polycrystalline (chert) | 0 | 0 | 0 | 0 | 0 | 0 | 0 | 0 | 0 | 0 | 0 | 0 | 0 | 0 |
| L—sedimentary | 0 | 0 | 0 | 17.4 | 17.6 | 17.7 | 13.9 | 23.1 | 20.8 | 25.4 | 23.8 | 0 | 0 | 0 |
| L—V | 0 | 100.0 | 100.0 | 82.6 | 82.4 | 82.3 | 86.1 | 76.9 | 79.2 | 74.6 | 76.2 | 100.0 | 100.0 | 100.0 |

Note: PA—Palen Mountains, MC—McCoy Mountains, DR—Dome Rock Mountains, N.D.—no data. Detrital modes are reported as percentages based on point count data from 600 grid points per thin section. Q—quartz, P—plagioclase, K—potassium feldspar, A—accessory minerals, l—indeterminate, L—lithic, and V—volcanic.

[†]Data in these columns are from McCoy Mountains Formation basal sandstone unit 1 of Harding (1982) and Harding and Coney (1985).

[§]Includes metavolcanic clasts.

[#]Includes metasedimentary clasts.

**Data available in Harding (1982) and Harding and Coney (1985).

nearby Cretaceous pluton. Another sample of the green ignimbrite yielded a K/Ar plagioclase age of 180 ± 3 Ma (Pelka, 1973; Stone and Pelka, 1989), but this age is too old and may thus reflect some combination of inherited and/or excess argon and argon loss (e.g., see Fleck et al., 1994). The U-Pb zircon dating method has proven far more appropriate for the dating of Jurassic metavolcanic rocks in California and Arizona because of the refractory nature of zircon, and its resistance to resetting by regional and contact metamorphism (Riggs et al., 1993).

However, the zircons are not free from complexity; their U-Pb systematics reflect not only igneous crystallization, but complex inheritance and later Pb loss. Inheritance comes from at least two sources: (1) zircons inherited from the source region of the magma, from magma chamber walls, and from walls of volcanic conduits; and (2) zircons entrained by ash flows as they flow

over the Earth's surface. Accordingly, we have designed our sample preparation and analytical techniques to deal with these problems, as discussed below. Another aspect of our approach to dating Jurassic metavolcanic rocks is that we sample only where numerous units in continuous stratigraphic order can be dated, in order to check for age consistency with respect to stratigraphic position (Busby-Spera et al., 1990a; Riggs et al., 1993; Fleck et al., 1994). We collected U-Pb zircon samples from four different units of the Dome Rock sequence in the Palen Mountains (in stratigraphic order: PA-17, PA-19, PA-12, and PA-8; see Figs. 1, 2, 3, and 7).

Analytical Methods

Zircon separates were prepared for the four samples by standard crushing, Wilfley table, heavy liquid, and magnetic separation methods.

Because most of the samples contain obvious entrained detrital components (frosted, rounded zircon grains), as well as euhedral magmatic zircons, the fractions were prepared for isotopic analysis by very careful hand picking in an attempt to isolate both relatively pure magmatic zircon fractions and pure detrital fractions.

Zircons were analyzed by a step-wise dissolution approach, following Mattinson (1984, 1994), in order to further assess the effects of inheritance and later Pb loss on the isotopic systematics of the zircons from these rocks. Our previous work has shown that this approach is highly effective in evaluating the effects of Pb loss associated with metamorphism of these Jurassic volcanic rocks (e.g., Busby-Spera et al., 1990a; Riggs et al., 1993). Some of the samples were initially analyzed by a simple two-step procedure, then later reanalyzed in more detail using three or four steps, or different time-temperature schedules

TABLE 2. (CONTINUED)

| Map unit Sample Number | Jm _{ms} | | | | | | Jm _{cg} | | | | | Jm _{cg} * | | |
|--------------------------------|------------------|-------|-------|-------|--------|-------|------------------|-------|-------|--------|--------|--------------------|-------|-------|
| | PA-11 | PA-12 | PA-15 | PA-16 | PA-33A | PA-61 | PA-19 | PA-26 | PA-30 | PA-33B | PA-37A | PA* | MC* | DR* |
| Petrographic Modes (%)† | | | | | | | | | | | | n = 2 | n = 6 | n = 7 |
| Monocrystalline rounded Q | 7.0 | 5.8 | 12.3 | 20.9 | 4.0 | 2.4 | 15.3 | 8.8 | 1.6 | 4.2 | 1.0 | ** | ** | ** |
| Monocrystalline angular Q | 37.0 | 24.4 | 40.1 | 40.7 | 58.8 | 86.4 | 44.7 | 62.6 | 41.8 | 53.2 | 52.0 | ** | ** | ** |
| Volcanic Q (embayed) | 1.2 | 0.3 | 5.0 | 0.4 | 0 | 0 | 0 | 0 | 0 | 0 | 0 | ** | ** | ** |
| P | 8.2 | 11.8 | 9.2 | 6.8 | 3.2 | 2.2 | 2.5 | 5.2 | 6.6 | 8.4 | 17.0 | ** | ** | ** |
| K | 2.2 | 1.8 | 2.4 | 0.6 | 0 | 0 | 0.7 | 0.8 | 0 | 1.8 | 4.0 | ** | ** | ** |
| A | 5.8 | 2.4 | 1.4 | 0.6 | 2.0 | 1.0 | 0.7 | 0.2 | 0.2 | 1.2 | 0.6 | ** | ** | ** |
| Monocrystalline I | 3.2 | 3.6 | 3.2 | 0.6 | 1.5 | 1.2 | 0.5 | 0.4 | 0.6 | 1.8 | 2.8 | ** | ** | ** |
| L—volcanic ^s | 12.8 | 18.6 | 8.4 | 15.8 | 4.7 | 0 | 0 | 0.8 | 0 | 1.2 | 0 | ** | ** | ** |
| L—sedimentary [#] | 1.6 | 2.9 | 0 | 0 | 2.7 | 2.2 | 4.3 | 8.0 | 2.6 | 6.4 | 3.0 | ** | ** | ** |
| L—tectonites | 0.0 | 0 | 2.4 | 1.8 | 3.3 | 0.2 | 8.1 | 3.0 | 6.2 | 4.6 | 8.8 | ** | ** | ** |
| L—hypabyssal | 4.6 | 6.8 | 0.4 | 0 | 0 | 0 | 0 | 0 | 8.4 | 2.4 | 0.0 | ** | ** | ** |
| L—I | 1.4 | 1.0 | 1.3 | 0.2 | 1.3 | 0.6 | 0.5 | 0.6 | 2.6 | 0.8 | 1.8 | ** | ** | ** |
| L—total | 20.4 | 29.3 | 12.5 | 17.8 | 12.0 | 3.0 | 12.9 | 12.4 | 19.8 | 15.4 | 13.6 | ** | ** | ** |
| % Interstitial Material | 15.0 | 20.6 | 13.8 | 11.6 | 18.5 | 3.8 | 22.7 | 9.6 | 29.4 | 14.0 | 9.0 | 16.0 | 7.0 | 9.0 |
| Total | 100.0 | 100.0 | 99.9 | 100.0 | 100.0 | 100.0 | 100.0 | 100.0 | 100.0 | 100.0 | 100.0 | | | |
| P/Total Feldspar | 0.8 | 0.9 | 0.8 | 0.9 | 1.0 | 1.0 | 0.8 | 0.9 | 1.0 | 0.8 | 0.8 | 1.0 | 1.0 | 1.0 |
| P (%Anorthite) | N.D. | N.D. | N.D. | N.D. | N.D. | N.D. | 25 | 15-60 | 54 | 30 | N.D. | N.D. | N.D. | N.D. |
| Qm F Lt Modes (%) | | | | | | | | | | | | | | |
| Q monocrystalline | 59.5 | 41.6 | 70.4 | 71.1 | 80.5 | 94.5 | 78.8 | 79.5 | 62.2 | 69.2 | 60.5 | 92.0 | 81.0 | 87.0 |
| Feldspar | 13.7 | 18.5 | 14.2 | 8.5 | 4.1 | 2.3 | 4.2 | 6.7 | 9.5 | 12.3 | 24.0 | 4.0 | 8.0 | 6.0 |
| L—total | 26.8 | 39.9 | 15.3 | 20.4 | 15.4 | 3.2 | 17.0 | 13.8 | 28.4 | 18.6 | 15.5 | 4.0 | 11.0 | 7.0 |
| L—(% by type) | | | | | | | | | | | | | | |
| V—felsitic | 28.2 | 41.9 | 49.5 | 83.3 | 40.0 | 0 | 0 | 6.5 | 0 | 7.8 | 0 | 0 | 0 | 1.0 |
| V—microlitic | 0 | 0 | 0 | 0 | 0 | 0 | 0 | 0 | 0 | 0 | 0 | 0 | 0 | 0 |
| V—lathwork | 0 | 0 | 0 | 0 | 0 | 0 | 0 | 0 | 0 | 0 | 0 | 0 | 0 | 0 |
| V—vitric | 34.5 | 28.0 | 12.3 | 5.5 | 0 | 0 | 0 | 0 | 0 | 0 | 0 | 0 | 0 | 0 |
| V—hypabyssal | 22.5 | 25.6 | 2.9 | 0 | 0 | 0 | 0 | 0 | 42.5 | 15.6 | 0 | 0 | 0 | 0 |
| Clastic—Q sericite | 7.9 | 0.7 | 0 | 0 | 13.7 | 62.8 | 33.3 | 48.4 | 13.1 | 20.9 | 22.1 | 100.0 | 86.0 | 79.0 |
| Orthoquartzite | 0 | 0 | 0 | 0 | 8.5 | 10.5 | 62.8 | 16.1 | 15.5 | 20.6 | 64.7 | 0 | 14.0 | 20.0 |
| Tectonite | 0 | 0 | 17.7 | 10.1 | 28.0 | 6.7 | 0 | 24.2 | 15.6 | 29.9 | 0 | 0 | 0 | 0 |
| L—I | 6.7 | 3.8 | 17.6 | 1.1 | 11.0 | 20.0 | 3.9 | 4.8 | 13.3 | 5.2 | 13.2 | 0 | 0 | 0 |
| QpLsLv Modes (%) | | | | | | | | | | | | | | |
| Q polycrystalline (chert) | 0 | 0 | 0 | 0 | 0 | 0 | 0 | 0 | 0 | 0 | 0 | 0 | 14.0 | 20.0 |
| L—sedimentary | 11.1 | 13.5 | 0 | 0 | 36.5 | 100.0 | 100.0 | 90.9 | 100.0 | 84.2 | 100.0 | 100.0 | 86.0 | 79.0 |
| L—V | 88.9 | 86.5 | 100.0 | 100.0 | 63.5 | 0 | 0 | 9.1 | 0 | 15.8 | 0 | 0 | 21.0 | 1.0 |

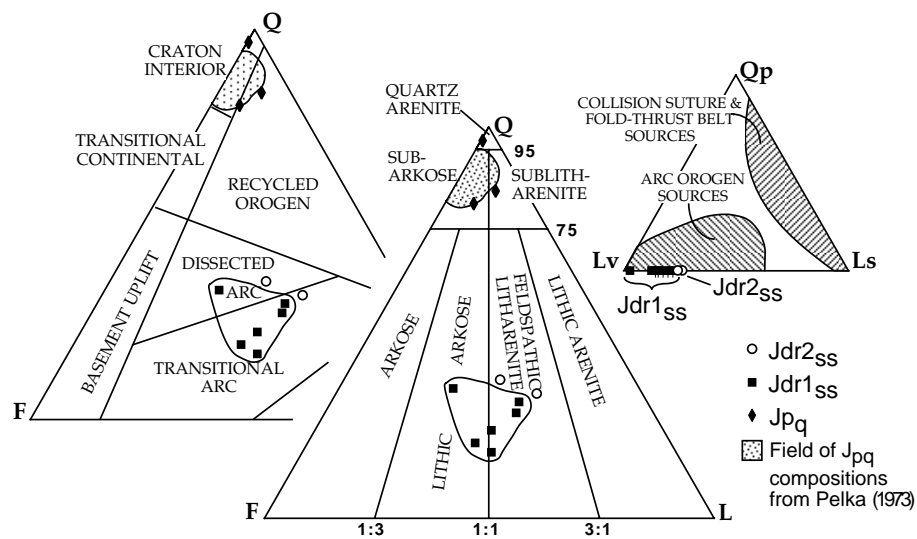


Figure 6. Petrographic classification (Folk, 1972) and provenance discrimination (Dickinson and Suczek, 1979; Dickinson et al., 1983) diagrams for samples from the upper Palen formation (Jp_q), the tuffaceous sandstone lithofacies (Jdr_{1ss}) of the basal volcaniclastic interval, and the sandstone-conglomerate lens (Jdr_{2ss}) of the middle rhyodacite unit of the Dome Rock sequence in the Palen Mountains, California. Note that data from the tuffaceous sandstone lithofacies (Jdr_{1ss}) plots in the dissected-transitional arc provenance fields. This is interpreted to result from admixture of mature sand from eolian dunes, now preserved as quartz arenite in the upper Palen formation (Jp_q) with the pyroclastic detritus of the basal volcaniclastic interval (Jdr_1). However, plotting the data on the polycrystalline lithic fragment ($QpLvLs$) discrimination diagram of Dickinson and Suczek (1979) removes the influence of the eolian sand and the data plot well within the arc orogen field.

TABLE 3. U-PB ISOTOPIC DATA FOR ZIRCON FRACTIONS FROM JURASSIC METAVOLCANIC UNITS, PALEN MOUNTAINS, CALIFORNIA

| Fraction type | Zircon size | Dissolution step ^{a-d†} | Fraction weight | Concentration | | Atomic ratios [§] | | | | Isotopic ratios [#] | | |
|-----------------------|-----------------------|------------------------------------------------------------------------|-----------------|-----------------------------------|-----------------------------------|---------------------------------------|------------------------------------------|---------------------------------------|------------------------------------------|----------------------------------|----------------------------------|---------------------------------------------|
| | | | | (ppm) | | ²⁰⁶ Pb/ ²⁰⁴ Pb | | ²⁰⁷ Pb/ ²⁰⁶ Pb* | | ²⁰⁶ Pb* | ²⁰⁷ Pb* | ²⁰⁷ Pb* |
| Sample ID | range | | (mg) | ²³⁸ U | ²⁰⁶ Pb* | ²⁰⁴ Pb | ²³⁸ U | ²³⁵ U | ²⁰⁶ Pb* | ²³⁸ U | ²³⁵ U | ²⁰⁶ Pb* |
| PA-17 Euhedral | | | | | | | | | | | | |
| PA-17 IA | 80-120μ | Residue Step ^c | 6.3 | 222.60 24.99 | 5.950 0.352 | 17903.0 29.7 | 0.03068 0.01567 | 0.2340 e | 0.05532 e | 194.8 104.1 | 213.5 e | 425±2 e |
| PA-17 IB | 80-120μ | Residue Step2 ^b Step1 ^a | 4.7 | 171.20 86.01 27.47 | 5.203 2.614 0.491 | 26191.0 3257.0 132.4 | 0.03509 0.03490 0.01767 | 0.2930 0.2926 0.1428 | 0.06055 0.06080 0.05863 | 222.3 221.1 113.0 | 260.9 260.6 135.6 | 623±2 632±3 553±75 |
| PA-17 VA | <80μ | Residue Step ^c | 5.7 | 272.40 45.46 | 7.332 0.686 | 27378.0 56.5 | 0.03108 0.01726 | 0.2394 e | 0.05586 e | 197.3 111.4 | 217.9 e | 447±2 e |
| PA-17 VB | <80μ | Residue Step2 ^b Step1 ^a | 4.1 | 175.20 110.90 40.64 | 4.963 3.186 0.615 | 26554.0 7078.0 232.8 | 0.03270 0.03311 0.01607 | 0.2570 0.2629 0.1156 | 0.05701 0.05759 0.05218 | 207.5 209.9 102.7 | 232.3 237.0 111.1 | 492±2 514±2 293±45 |
| PA-17 IX | <80μ Fine Tap | Residue Step2 ^b Step1 ^a | 3.1 | 183.40 130.17 44.82 | 5.334 3.913 0.697 | 16814.0 12207.0 223.6 | 0.03357 0.03468 0.01645 | 0.2700 0.2851 0.1205 | 0.05854 0.05963 0.05319 | 212.9 219.8 105.1 | 242.7 254.7 115.5 | 542±2 570±2 337±50 |
| PA-17 Rounded | | | | | | | | | | | | |
| PA-17 II | 80-120μ | Residue Step ^a | 1.4 | 164.30 38.42 | 14.901 0.468 | 9255.0 201.4 | 0.10459 0.01276 | 1.2213 0.0701 | 0.08467 0.05120 | 641.3 81.7 | 810.4 87.6 | 1308±2 250±60 |
| PA-17 III | 80-120μ | Residue Step ^a | 1.5 | 340.30 50.92 | 47.090 1.069 | 47780.0 114.8 | 0.15978 0.02025 | 2.1410 0.1677 | 0.09719 0.06006 | 955.6 129.2 | 1162.2 157.4 | 1571±2 606±90 |
| PA-17 IV & VIII | >120μ | Residue Step ^a | 0.3 | 434.60 63.06 | 36.410 1.587 | 17433.0 294.9 | 0.09668 0.02721 | 1.0683 0.2125 | 0.08014 0.05664 | 594.9 173.1 | 737.9 195.6 | 1200±2 478±50 |
| PA-17 VI | <80μ | Residue Step ^a | 2.3 | 252.30 63.49 | 14.660 0.835 | 20503.0 285.9 | 0.06707 0.01419 | 0.7034 0.1027 | 0.07606 0.05250 | 418.5 90.8 | 540.8 94.3 | 1097±2 307±40 |
| PA-17 VII | <80μ | Residue Step ^a | 1.8 | 403.40 66.20 | 49.480 1.437 | 57443.0 368.2 | 0.14168 0.02379 | 1.7340 0.2040 | 0.08877 0.06218 | 854.0 151.6 | 1021.0 188.5 | 1399±2 680±25 |
| PA-12 Euhedral | | | | | | | | | | | | |
| PA-12 IA | <80μ | Residue Step 2 ^b Step1 ^a | 3.9 | 205.30 431.10 94.99 | 4.750 10.776 2.241 | 23597.0 14591.0 145.7 | 0.02672 0.02887 0.02726 | 0.1889 0.2024 0.1923 | 0.05128 0.05084 0.05115 | 170.0 183.5 173.4 | 175.7 187.1 178.6 | 253±2 234±2 248±75 |
| PA-12 IB | <80μ | Residue Step3 ^d Step2 ^c Step1 ^a | 0.8 | 510.70 36.74 42.24 50.57 | 11.281 0.732 0.873 1.007 | 47420.0 1924.0 3013.0 1589.0 | 0.02552 0.02303 0.02388 0.02301 | 0.1764 0.1590 0.1654 0.1575 | 0.05012 0.05007 0.05023 0.04965 | 162.5 146.8 152.2 146.6 | 164.9 144.8 155.4 148.5 | 200.5±1 198.2±12 205.6±9 178±19 |
| PA-12 IIIA | 80-120μ fine tap | Residue Step 2 ^b Step1 ^a | 4.9 | 206.90 281.30 72.91 | 4.712 7.402 1.766 | 20270.0 8598.0 191.8 | 0.02630 0.02977 0.02797 | 0.1881 0.2152 0.2104 | 0.05186 0.05244 0.05455 | 167.4 189.1 178.0 | 175.0 197.9 193.9 | 279±2 305±2 394±50 |
| PA-12 IIIB | 80-120μ fine tap | Residue Step3 ^d Step2 ^c Step1 ^a | 0.5 | 445.30 23.36 33.72 33.16 | 9.934 0.476 0.661 0.657 | 38244.0 1146.0 2105.0 828.6 | 0.02578 0.02354 0.02266 0.02288 | 0.1780 0.1616 0.1558 0.1558 | 0.05009 0.04980 0.04987 0.04939 | 164.1 150.0 144.5 145.8 | 166.4 152.1 147.0 147.0 | 199.1±1 185.6±24 188.9±17 166.3±25 |
| PA-12 VA | 80-120μ coarse tap | Residue Step 2 ^b Step1 ^a | 4.1 | 220.50 235.40 41.76 | 50.308 5.745 1.051 | 13330.0 10930.0 83.1 | 0.02636 0.02820 0.02910 | 0.1877 0.2023 0.2217 | 0.05164 0.05202 0.05526 | 167.7 179.3 185.0 | 174.7 187.0 203.0 | 270±2 286±2 423±145 |
| PA-12 VB | 80-120μ coarse tap | Residue Step3 ^d Step2 ^c Step1 ^a | 1.6 | 403.50 12.88 24.05 17.30 | 9.806 0.278 0.495 0.348 | 48600.0 2872.0 2922.0 865.0 | 0.02807 0.02498 0.02377 0.02322 | 0.2093 0.1820 0.1718 0.1659 | 0.05408 0.05285 0.05242 0.05183 | 178.4 159.0 151.4 148.0 | 193.0 169.8 161.0 155.9 | 374.3±1 322.3±11 303.7±12 277.9±16 |
| PA-12 VII | >120μ | Residue Step 2 ^b Step1 ^a | 2.7 | 188.00 160.40 19.53 | 4.509 3.927 0.430 | 18571.0 2078.0 64.8 | 0.02771 0.02828 0.02540 | 0.2036 0.2105 0.1910 | 0.05330 0.05399 0.05453 | 176.2 179.8 161.7 | 188.2 194.0 177.5 | 342±2 371±5 393±200 |
| PA-12 Rounded | | | | | | | | | | | | |
| PA-12 II | <120μ frosted | Residue Step ^a | 0.5 | 562.70 49.54 | 14.575 1.089 | 7839.0 86.9 | 0.02994 0.02540 | 0.2397 0.1826 | 0.05806 0.05215 | 190.1 162.0 | 218.2 170.0 | 532±3 292±150 |
| PA-8 Euhedral | | | | | | | | | | | | |
| PA-8 V | 120-165μ | Residue Step ^a | 9.5 | 480.40 30.90 | 11.110 0.572 | 10014.0 566.0 | 0.02668 0.02067 | 0.1966 0.1438 | 0.05345 0.05046 | 169.7 131.9 | 182.3 136.4 | 348±1 216±23 |
| PA-8 VI | 80-120μ | Residue Step ^a | 0.5 | 217.13 22.17 | 4.880 0.432 | 3227.0 358.0 | 0.02583 0.02136 | 0.1779 0.1453 | 0.04996 0.04935 | 164.4 136.2 | 166.3 137.8 | 193±4 164±37 |
| PA-8 VII | >165μ | Residue Step ^a | 0.2 | 245.90 15.07 | 5.945 0.363 | 2650.0 311.0 | 0.02773 0.02614 | 0.1912 0.1819 | 0.05002 0.05047 | 176.3 166.3 | 177.7 169.7 | 196±5 217±41 |

Note: all samples nonmagnetic in Frantz magnetic separator at 1° side tilt, 16° forward tilt, and 1.5 amps. e indicates that ²⁰⁷Pb*/²³⁵U and ²⁰⁷Pb*/²⁰⁶Pb* ratios and ages were not calculated due to extremely low ²⁰⁶Pb*/²⁰⁴Pb values.

*Denotes radiogenic isotopes.

Stepwise dissolution procedure as described in Mattinson (1984, 1994). Superscripts a–d designate different dissolution schedules: a = 24 hr at 80 °C, b = 24 hr at 166 °C, c = 5 days at 80 °C, d = 10 days at 80 °C.

§Corrected for 0.125% mass fractionation on the basis of multiple replicate analyses of National Institute of Standards and Technology Pb and U standards.

#Decay constants used: ²³⁵U = 9.8485 x 10E-10; ²³⁸U = 1.55125 x 10E-10; ²³⁸U/²³⁵U = 137.88. Combined sources of error of ²⁰⁶Pb*/²³⁸U age include error propagated in measurements of individual isotopes and assessment of error on initial ²⁰⁶Pb*/²⁰⁴Pb. ²⁰⁶Pb*/²³⁸U ages estimated to have ±1% error (~2 m.y.) except where noted. Uncertainties in ²⁰⁷Pb*/²⁰⁶Pb* ages is based on error in measured ²⁰⁶Pb*/²⁰⁴Pb (<0.09%) and on initial ²⁰⁷Pb*/²⁰⁴Pb values. See Mattinson (1987, 1994) and text for discussion of sources and propagation of error.

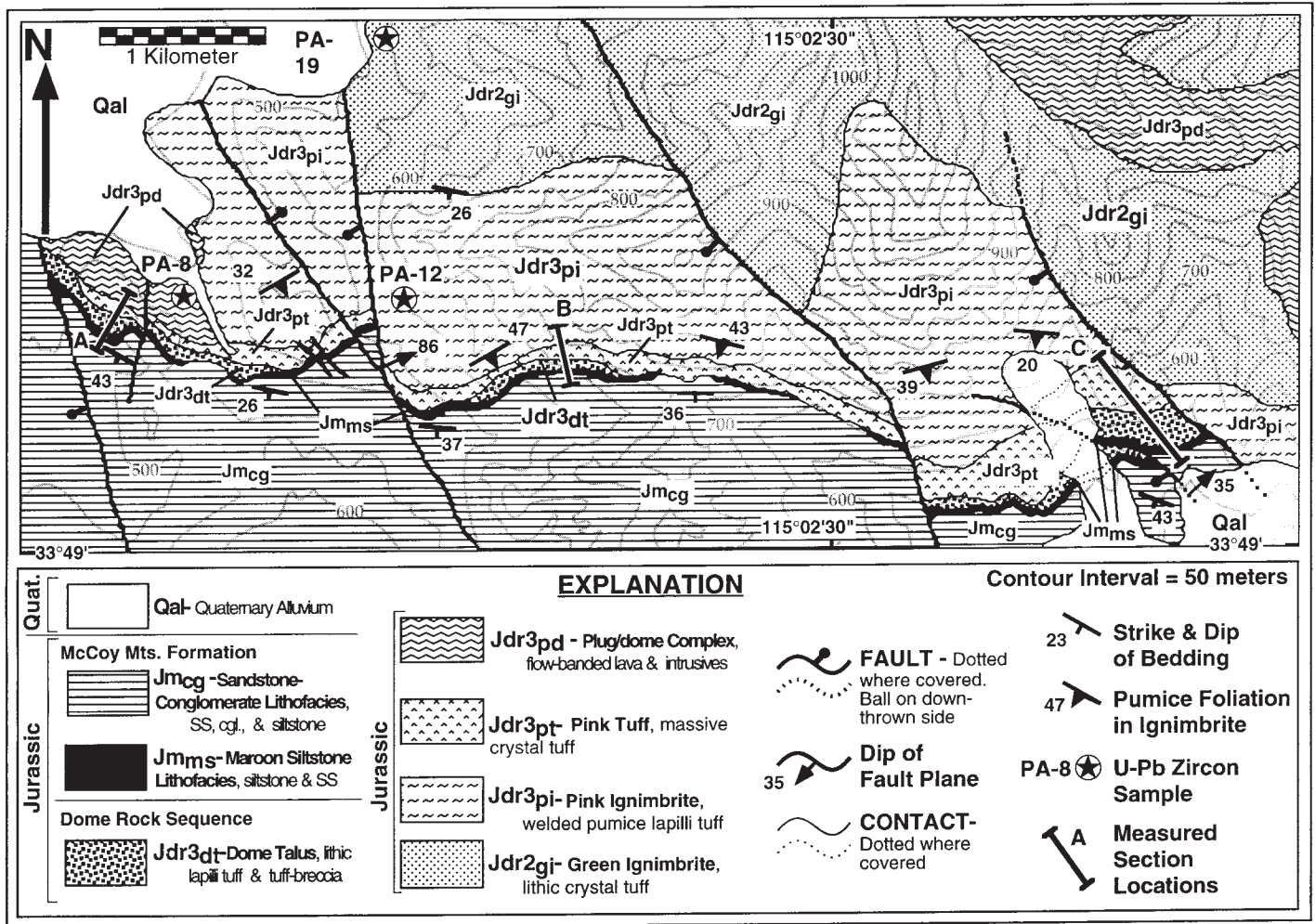


Figure 7. Geologic map of the contact between the Dome Rock sequence and overlying McCoy Mountains Formation (the location of map is shown in Fig. 1b). Stratigraphic top is to the south. Locations of the U-Pb zircon samples (PA-19, PA-12, and PA-8) are shown by stars. Locations of the three measured sections shown in Figure 8 are designated by the lines labeled A, B, and C. The topography is shown in gray.

(see Table 3), selected on the basis of the initial results. The isotopic data for the individual steps, plus details of the partial dissolution schedules and uncertainties in the calculated ages are provided in Table 3. The results are plotted on Tera-Wasserburg diagrams in Figures 10 and 11. Intercept ages, uncertainties, and mean standard weighted deviates (MSWD) are from the regression program of Ludwig (1991), using his Model 1 except where noted.

Error Analysis

Summing the effects of measurement error, initial lead estimation error, and a conservative allowance for any possible disequilibrium effects during step-wise dissolution indicates a maximum uncertainty of ± 2 m.y. for $^{238}\text{U}/^{206}\text{Pb}$ * ages. Uncertainty in $^{207}\text{Pb}/^{206}\text{Pb}$ * ages is based on error in measured $^{207}\text{Pb}/^{206}\text{Pb}$, $^{206}\text{Pb}/^{204}\text{Pb}$ ratios,

and on uncertainty in the initial $^{207}\text{Pb}/^{204}\text{Pb}$ ratios. Error analysis follows the procedure of Mattinson (1987) and Ludwig (1991). All uncertainties are stated at the 2s level. All the MSWD are greater than one (>1), indicating scatter outside our analytical errors (i.e., geologic scatter) probably related to a range in the ages of inherited material. This means that the upper intercept is an "average" value reflecting a combination of older and younger inherited zircon, and introduces a larger uncertainty into the lower intercept than would occur if the inherited material was from one source. However, this geologic scatter should not systematically affect the lower intercepts (e.g., shifting them all to older or younger ages). This effect can be mitigated by using model 2 of Ludwig (1991), which assigns equal weights and zero error correlation to each data point. Application of this model is justified when geologic scatter is greater than analytical error as

is the case with the rounded (inherited and possibly detrital) zircons from sample PA-17.

Analytical Results

Sample PA-17 was collected from the lapilli tuff (Jdr1_{lt}, Figs. 2 and 4). The sample yielded 10 zircon fractions differentiated on the basis of size and shape (clear-euhedral and rounded morphologies). The fractions were subjected to step-wise partial dissolution and analysis utilizing two or three steps (Table 3). Regression through points from data for clear euhedral zircon residues and final dissolution steps defines a lower intercept at 174 ± 8 Ma and an upper intercept of 1507 ± 168 Ma (Fig. 10) with a MSWD of 5.6. The lower intercept is interpreted to represent a Middle Jurassic emplacement age for the pyroclastic deposits of the lapilli tuff (Jdr1_{lt}) (Fig. 12). The upper intercept is a reasonable

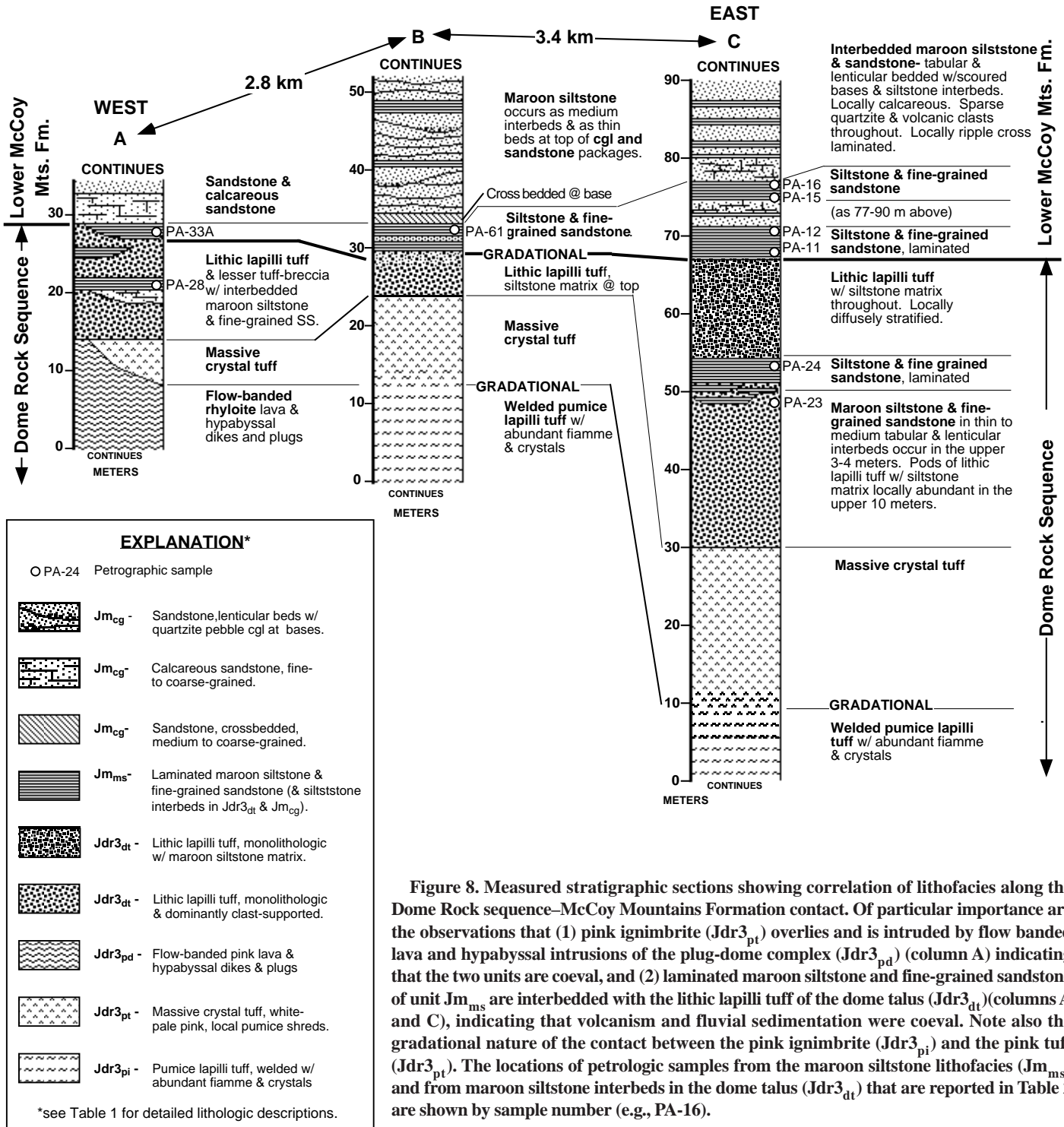


Figure 8. Measured stratigraphic sections showing correlation of lithofacies along the Dome Rock sequence–McCoy Mountains Formation contact. Of particular importance are the observations that (1) pink ignimbrite ($Jdr3_{pt}$) overlies and is intruded by flow banded lava and hypabyssal intrusions of the plug-dome complex ($Jdr3_{pd}$) (column A) indicating that the two units are coeval, and (2) laminated maroon siltstone and fine-grained sandstone of unit Jm_{ms} are interbedded with the lithic lapilli tuff of the dome talus ($Jdr3_{dt}$) (columns A and C), indicating that volcanism and fluvial sedimentation were coeval. Note also the gradational nature of the contact between the pink ignimbrite ($Jdr3_{pi}$) and the pink tuff ($Jdr3_{pt}$). The locations of petrologic samples from the maroon siltstone lithofacies (Jm_{ms}) and from maroon siltstone interbeds in the dome talus ($Jdr3_{dt}$) that are reported in Table 2 are shown by sample number (e.g., PA-16).

“average” age for basement-derived zircon cores in the euhedral zircons from Precambrian rocks in the region, which range in age from ~1.8 Ga to ~1.4 Ga (Condie, 1982; Anderson, 1983; Nelson and DePaolo, 1985; Anderson, 1989).

Inclusion of data from the rounded zircon fractions in a regression calculation using model 2 of Ludwig (1991) produces the same lower inter-

cept (within error) but with much larger confidence limits. We interpret this large scatter to reflect derivation of the rounded zircons from a variety of sources, including the basement rocks through which the parent magma intruded, and detrital zircons from the eolian sands on which the lapilli tuff was transported and emplaced.

Sample PA-19 was collected from approxi-

mately 200 m below the top of the green ignimbrite ($Jdr2_{gi}$, Figs. 2 and 7). The sample yielded five zircon fractions, distinguished on the basis of size and morphology, that were analyzed using two dissolution steps. These data were reported and interpreted by Busby-Spera et al. (1990a). Here, however, we have reanalyzed the data using the regression algorithms of Ludwig (1991).

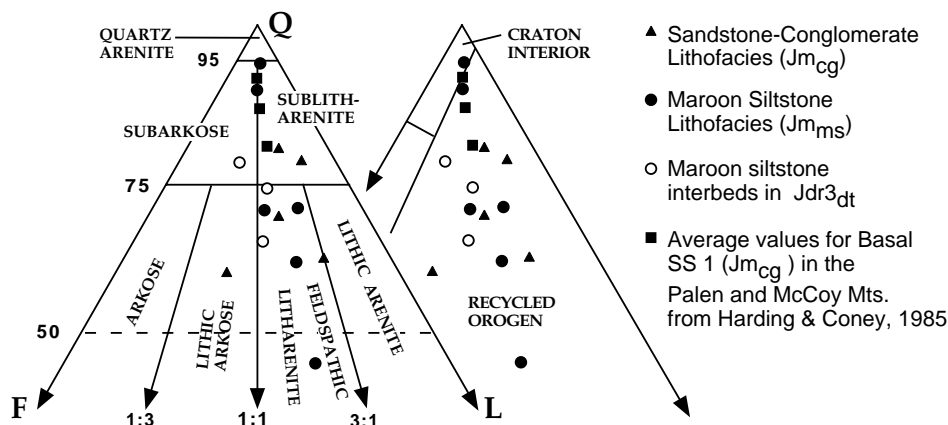


Figure 9. Petrographic classification (Folk, 1972) and provenance discrimination (Dickinson and Suczek, 1979, Dickinson et al., 1983) diagrams for the maroon siltstone lithofacies (Jm_{ms}) and the sandstone-conglomerate lithofacies (Jm_{cg}) of the basal McCoy Mountains Formation. Note the relatively mature nature of some of the samples (subarkose and sublitharenites), reflecting a large component of craton-derived sediment. This suggests that craton-derived detritus, possibly equivalent to the Entrada Sandstone (see Fig. 12), may have had access to this segment of Mesozoic continental arc during deposition of the basal McCoy Mountains Formation.

Regression through points from data for zircon residue defines a lower intercept at 155 ± 8 Ma and an upper intercept of 1368 ± 429 Ma (Fig. 10) with an MSWD of 13. The lower intercept is interpreted as the emplacement age for the green ignimbrite ($Jdr2_{gi}$). The upper intercept reflects inheritance from basement rocks.

Sample PA-12 was collected from near the top of the pink ignimbrite ($Jdr3_{pi}$, Figs. 2 and 7). The sample yielded eight fractions of zircon, distinguished on the basis of size and morphology, that were analyzed using three or four dissolution steps (Table 3). Regression through points from data for zircon residue and the last partial dissolution step define a lower intercept at 162 ± 3 Ma and an upper intercept of 1622 ± 189 Ma (Fig. 11) with an MSWD of 5.4. The lower intercept is interpreted as the emplacement age of the pink ignimbrite ($Jdr3_{pi}$). This age is indistinguishable from that of the underlying green ignimbrite (sample PA-19), within analytical error. The upper intercept reflects inheritance from basement rocks.

Sample PA-8 was collected from the plug-dome complex ($Jdr3_{pd}$, Figs. 2 and 7). The sample yielded three euhedral zircon fractions, distinguished on the basis of size, that were analyzed using two dissolution steps (Table 3). Data for zircon residue are scattered on the Tera-Wasserburg diagram (Fig. 11), and are difficult to interpret. Data from the two fractions of smaller euhedral zircons (fractions 1 and 2) fall very close to the trajectory defined by fractions from sample PA-12 (pink ignimbrite [$Jdr3_{pi}$], Fig. 11), suggesting that the two units are of similar age. This interpretation of the isotopic data is sup-

ported by field relations (described above), which indicate that the pink ignimbrite ($Jdr3_{pi}$) and plug-dome complex ($Jdr3_{pd}$) are coeval. If this is correct, fraction 3 might reflect inheritance of zircon from units deeper in the stratigraphic succession (e.g., unit $Jdr1_{it}$, Fig. 11). Thus, the fraction 3 zircons are only slightly older than the emplacement age of the plug-dome complex, in contrast to the predominantly Proterozoic age of most inherited zircons analyzed by this study. An alternative interpretation of the isotopic data is that PA-8 zircons are older than those of PA-12; fractions 1 and 2 exhibited apparent lowering in age due to late Pb loss that was not removed by the partial dissolution approach used in analyzing these samples. This interpretation, however, is contradicted by field relations.

DISCUSSION

Our U-Pb zircon data, field mapping, and volcanic and sedimentary facies analysis indicate that in the Palen Mountains, the upper Palen formation, Dome Rock sequence, and lower McCoy Mountains Formation comprise a conformable stratigraphic section spanning at least late Middle Jurassic through early Late Jurassic time and probably longer (Fig. 12). Preservation of this approximately 7.5-km-thick section required protracted and relatively rapid subsidence. Uncertainties in the U-Pb zircon data permit subsidence rates between 1.1 km/m.y. and 0.2 km/m.y. during the accumulation of this conformable section. This is consistent with the interpretation of Reynolds et al. (1989) that the Late Triassic to Middle Jurassic uplift in south-

eastern California and western Arizona, which preceded the main phase of arc magmatism, had ceased by Middle Jurassic time. Middle Jurassic to early Late Cretaceous subsidence, represented in part by the Palen Mountain section, was followed by intense latest Mesozoic contractional deformation (Reynolds et al., 1987).

Age and Correlation of the Upper Palen Formation Eolianite

The 174 ± 8 Ma U-Pb zircon age of the basal Dome Rock sequence ($Jdr1$, PA-17, Fig. 12) in the Palen Mountains indicates a Middle to late Early Jurassic (Toarcian to Bathonian) age for the upper part of the eolianite (Jp_q) in the Palen formation. The data permit age correlation of the upper part of the eolianite (Jp_q) with the Bajocian-Bathonian Page Sandstone of north-central Arizona and south-central Utah, the scattered eolian deposits of the Bajocian-Bathonian Carmel Formation of north-central Arizona and southern Utah, or at the lowermost limit of U-Pb zircon data uncertainty, the Aalenian-Bajocian Temple Cap Sandstone of southwestern Utah (Fig. 12). These age correlations are based on the stratigraphy synthesized in Blakey et al. (1988) and the time scale of Gradstein et al. (1994).

The depositional characteristics and distribution of eolian facies of the Page Sandstone, Carmel Formation, and Temple Cap Sandstone are equivocal in distinguishing between these potential correlatives.

Page Sandstone. The Page Sandstone is considered to be the erosional remnant of an erg that extended farther west than the present westward outcrop limit in south-central Utah and north-central Arizona (Blakey et al., 1988; Chan and Kocurek, 1988). Eolianites of the Page Sandstone are thickest at this southwestern limit of exposure; to the south they have been removed by erosion (Blakey et al., 1988). Thus, although a present-day ~370–390-km gap exists between quartz arenites of the Page Sandstone and of the upper Palen formation (once ~60 km of Cenozoic extension across the Colorado extensional corridor are removed; Spencer and Reynolds, 1989; Howard and John, 1987), the Page Sandstone erg possibly extended considerably farther to the southwest, into the arc orogen.

Carmel Formation. The Carmel Formation overlies and is in part the lateral equivalent of the Page Sandstone (Fig. 12). It contains scattered eolian deposits that occur principally along the Utah-Arizona border (Blakey et al., 1988). Although these eolian deposits are minor in volume when compared with the Page Sandstone or Temple Cap Sandstone, their age and distribution require that they be considered as possible correlatives of the eolianite in the upper Palen formation. Age correlation of eolianite of the upper

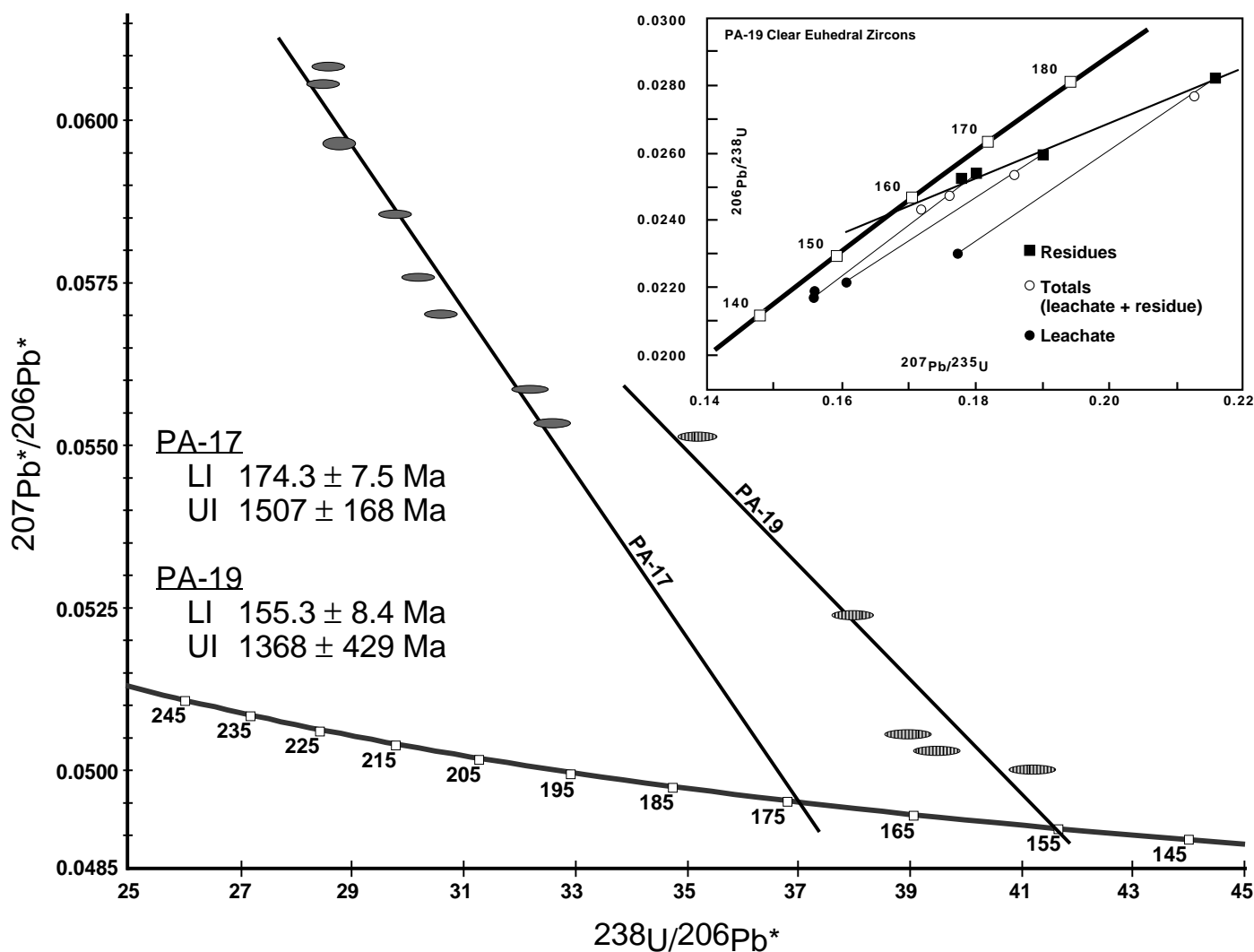


Figure 10. Enlarged portion of the Tera-Wasserburg concordia diagram showing isotopic data from U-Pb zircons samples PA-17 and PA-19. The concordia curve plots through the small open squares. PA-17 data are from residues of five euhedral zircon fractions and from the last dissolution steps of the three fractions on which multiple dissolution steps were performed (IB, VB, and IX). Data from rounded zircons were not included in the regression because geological scatter in these fractions produced huge errors (MSWD = 1260; see text). PA-19 data (previously published; Busby et al., 1990a) are from residues of five fractions from the green rhyodacite ignimbrite (Jdr2_{gt}). The inset shows a concordia diagram for dissolution step (solid circles), residue (solid squares), and total (dissolution step ± residue) (open circles) data from four fractions of clear euhedral zircons from the sample PA-19. The coarsest fractions plot on the upper right side of the diagram, and the finest are shown at the lower left. The lines connect dissolution step, residue, and total data for individual fractions. The chord defining the lower intercept is plotted through the residue data. This plot clearly shows the effectiveness of the step-wise dissolution technique at removing the effects of lead loss. Only four fractions are shown for legibility. Isotopic data for all fractions are tabulated in Table 3.

Palen formation with those of the Carmel Formation is supported by ⁴⁰Ar/³⁹Ar ages on bentonites collected from several stratigraphic horizons of the Carmel Formation (Everett et al., 1989; B. Kowallis, 1991, personal commun.).

Temple Cap Sandstone. The current outcrop distribution of eolian quartz arenite of the Temple Cap Sandstone is limited to southwestern Utah. Arguments based on the relationship between sea level and basinward erg extent suggest that the present outcrop distribution of the Temple Cap Sandstone is a small remnant of a larger erg that

originally extended farther westward (Chan and Kocurek, 1988) and possibly southward. Paleocurrent data indicate southward-dominant wind directions (Blakey et al., 1988). The Temple Cap Sandstone is truncated toward the south, in the direction of the Palen Mountains, by the sub-Cretaceous unconformity (Blakey et al., 1988). Therefore, an approximately 290–320-km gap exists between quartz arenites of the Temple Cap Sandstone and of the upper Palen formation (correcting for Tertiary extension). These paleogeographic considerations indicate that, in the

context of the chronostratigraphic synthesis of Blakey et al. (1988) and the time scale of Gradstein et al. (1994), the eolianites of the upper Palen formation may be correlative with the Temple Cap Sandstone (Fig. 12).

Navajo Sandstone. Our data from the upper part of the eolianite (Jp₁) in the upper Palen formation do not preclude the age correlation made by previous workers with the Early Jurassic (Pliensbachian-Toarcian) Aztec–Navajo Sandstones (Marzolf, 1980; Hamilton, 1987) (Fig. 12). This seems unlikely, however, because it requires

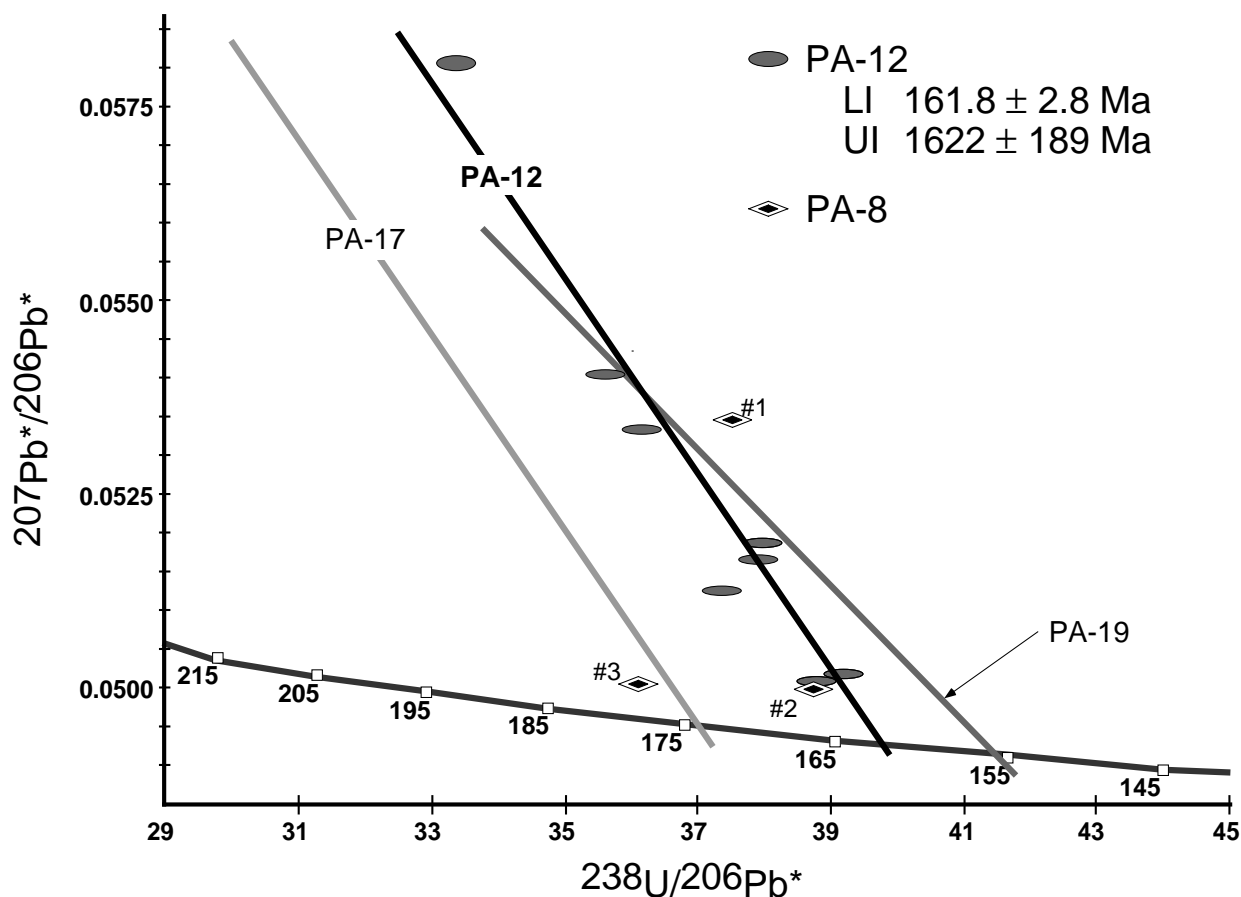


Figure 11. Enlarged portion of the Tera-Wasserburg concordia diagram showing U-Pb zircon isotopic data for samples PA-8 ($Jdr3_{pd}$) and PA-12 ($Jdr3_{pi}$). The concordia curve plots through the small open squares. Discordia trajectories for samples PA-17 and PA-19 are shown in gray for reference. PA-12 data are from residues of seven euhedral zircon fractions and one rounded zircon fraction. The three zircon fractions from sample PA-8 ($Jdr3_{pd}$) are also shown. Although PA-8 data are difficult to interpret due to significant scatter, two of the fractions (1 and 2) have ages close to those of fractions from sample PA-12 ($Jdr3_{pi}$), with which it appears to be coeval on the basis of field relations. The third PA-8 fraction (3) appears to be the same age as PA-17, suggesting that the rhyolite magma of the plug-dome complex ($Jdr3_{pd}$) may have incorporated zircons from the basal volcanoclastic interval ($Jdr1$) during its intrusion and eruption. Isotopic data for all fractions are tabulated in Table 3.

assuming the maximum error on both the U-Pb zircon age (174 ± 8 Ma) and on uncertainties in the absolute ages of the stage boundaries (± 4 Ma) (Fig. 12). These assumptions would result in an overlap of only one million years between the Navajo Sandstone and our date constraining the age of the upper Palen formation.

The likelihood that craton-derived eolian sands other than those of the Early Jurassic Navajo–Aztec erg commingled with pyroclastic detritus of the Jurassic arc is significant because it indicates that the arc was low standing in Middle Jurassic time. This supports the interpretation that on a regional scale, the arc was a long lived (~ 35 m.y.) trap for craton-derived sands (Busby-Spera, 1988; Riggs et al., 1993).

Age of the Dome Rock Sequence

Previous to this study, the Dome Rock sequence was very sparsely dated. Our U-Pb zircon date of 175 ± 8 Ma from sample PA-17 of

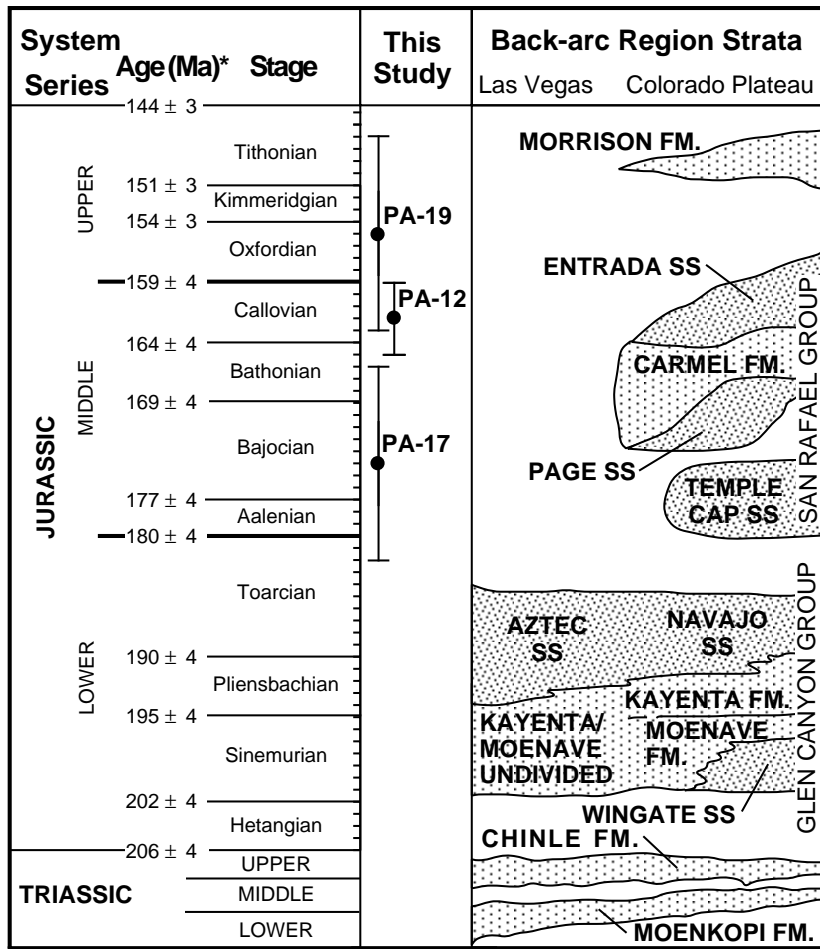
the basal volcanoclastic interval ($Jdr1$) is the oldest date reported from the Dome Rock sequence. Taken together, our U-Pb zircon data (Figs. 10, 11, and 12; Table 3) constrain Mesozoic volcanism in the Palen Mountains to being younger than Early Jurassic (Toarcian) and older than Early Cretaceous (Berriasian). Comparison of published U-Pb zircon data for the Dome Rock sequence with our new data indicates that the upper portion of the Dome Rock sequence in the Palen Mountains is age correlative with the Planet and Black Rock volcanic rocks of western Arizona (Reynolds et al., 1987) and broadly correlative with other sparsely dated portions of the Dome Rock sequence (L. T. Silver *in* Crowl, 1979; Tosdal, 1986).

Age and Correlation of the Lower McCoy Mountains Formation

The contact between the Dome Rock sequence and the McCoy Mountains Formation is con-

formable and interfingering. This is significant because our U-Pb zircon data from the green ignimbrite ($Jdr2_{gi}$), the pink ignimbrite ($Jdr3_{pi}$), and the plug-dome complex ($Jdr3_{pd}$) also constrain the age of the basal strata of the McCoy Mountains Formation. Therefore the 155 ± 8 Ma and 162 ± 3 Ma dates from the green ignimbrite ($Jdr2_{gi}$) and the pink ignimbrite ($Jdr3_{pi}$) indicate a latest Middle Jurassic to Late Jurassic (Callovian-Tithonian) age range for the basal McCoy Mountains Formation.

The age constraints on the basal McCoy Mountains Formation allow its correlation with two other regionally significant units. The submaturation (very quartz rich) nature of sandstones in the basal McCoy Mountains Formation (Fig. 9, Table 2) suggests possible distal equivalence to the Entrada Sandstone of southwestern Utah (Fig. 12). This is significant because it means that craton-derived detritus may have had access to the Mesozoic continental arc at this site from Middle to Late Jurassic time. Our new age constraints on the lower



*Stage boundaries: Gradstein et al., 1994

Figure 12. Composite stratigraphic chart showing age ranges of lower Mesozoic eolian sandstones of the southwestern United States (from Blakey et al., 1988) and U-Pb zircon ages for the Dome Rock sequence (this study). The ages of stages are from Gradstein et al. (1994). Uncertainties in the ages of stage boundaries are ±4 m.y. for Middle Jurassic and ±3 m.y. for Late Jurassic time. It should also be noted that the absolute ages of the stratigraphic units on the Colorado Plateau also have large uncertainties. Modified from Blakey et al. (1988) and from Riggs et al. (1993).

McCoy Mountains Formation also strengthen its correlation with the basal strata of the Bisbee Group of southeastern Arizona and northern Mexico. These basal strata, informally referred to as the Glance conglomerate, have been interpreted as either arc related (Tosdal et al., 1989) or rift related (Dickinson et al., 1986), and comprise piedmont fan deposits with interbedded ignimbrites and lava flows in grabens, half grabens, and calderas (Bilodeau and Keith, 1979; Dickinson et al., 1987; Busby-Spera and Kokelaar, 1991, 1992; Lipman and Hagstrum, 1992; Basset and Busby, 1996). Our U-Pb zircon data constraining the age of the lower McCoy Mountains Formation indicate that opening of the McCoy basin was concurrent with opening of the Bisbee basin, within the limits of sparse isotopic data for the Bisbee Group (see ref-

erences in Busby-Spera et al., 1990a; Saleeby and Busby, 1992).

Plate-Margin-Scale Reconstructions

Jurassic rocks of western North America chronicle complex magmatic and tectonic events reflecting the entire range of strain regimes, from highly extensional to highly compressional (e.g., articles in Miller and Busby, 1995). The available data from California, Arizona, and Nevada suggest that the length of the arc-backarc region was dominated by extension from its Triassic inception through early Middle Jurassic time (Busby-Spera et al., 1990a, 1990b) and appears to have occupied a nearly continuous arc graben depression, more than 1000 km long (Busby-Spera,

1988). The Middle Jurassic eolianite (Jp_q) in the Palen Mountains may have been deposited in a basin within this tectonic regime.

By late Middle to Late Jurassic time, the Klamath-Sierran and Mojave-Sonoran segments of the arc became dissimilar in their overall tectonic setting (Busby-Spera et al., 1990a, 1990b). This complexity has been interpreted to be the result of a strong tangential component of relative motion along the North American plate margin, as described by Saleeby and Busby-Spera (1992; see references therein). Sinistral transpressive deformation of the northern part of the arc (Fig. 13) resulted in the classic Nevadan orogeny of the Sierra Nevada, as well as backarc contractile deformation in northwest Nevada, and sinistral strike-slip faults cutting the forearc to backarc regions. Sinistral transtension in the southern part of the arc (Fig. 13) resulted in displacements of perhaps several hundred kilometers in Mexico (Silver and Anderson, 1974), and emplacement of dike swarms from the Sonoran to eastern Sierra Nevada regions (Saleeby and Busby-Spera, 1992). Sinistral faulting may have also operated during the rift phase in the evolution of the Bisbee basin in southern Arizona, the opening of which has been attributed to exploitation of the thermally weakened welt of the Jurassic continental arc by Gulf of Mexico-related rifting (Dickinson et al., 1987; Busby-Spera et al., 1989). Saleeby and Busby-Spera (1992) proposed that the broad relationship between sinistral faulting in Cordilleran and Atlantic margin tectonics, as suggested by Dickinson et al. (1987), resulted from the large northwest component of absolute motion reported at this time for North America by May et al. (1989).

This study demonstrates for the first time that (1) the initiation of the McCoy basin was synchronous with that of the Bisbee basin, and (2) like the Bisbee basin, Upper Jurassic strata of the McCoy basin record a waning of volcanism and the initial accumulation of thick clastic sequences. We speculate that this indicates that the two basins are tectonically related, even though they are geographically distinct (Fig. 13). Further work is needed to determine whether or not they are linked by Late Jurassic faults. We also speculate that differences between the two basins reflect along-strike variation in plate-margin orientation. In contrast to the coeval Bisbee Group, rugged relief and unroofing of the Jurassic arc are not indicated by the stratigraphy and petrology of the lower McCoy Mountains Formation, nor are its basal deposits dominantly coarse grained (Harding and Coney, 1985; Saleeby and Busby-Spera, 1992). Furthermore, the volcanic to sedimentary transition is much more abrupt in the McCoy basin than it is in the Bisbee basin (Adams et al., 1991). Clearly, tectonic subsidence was required during deposition

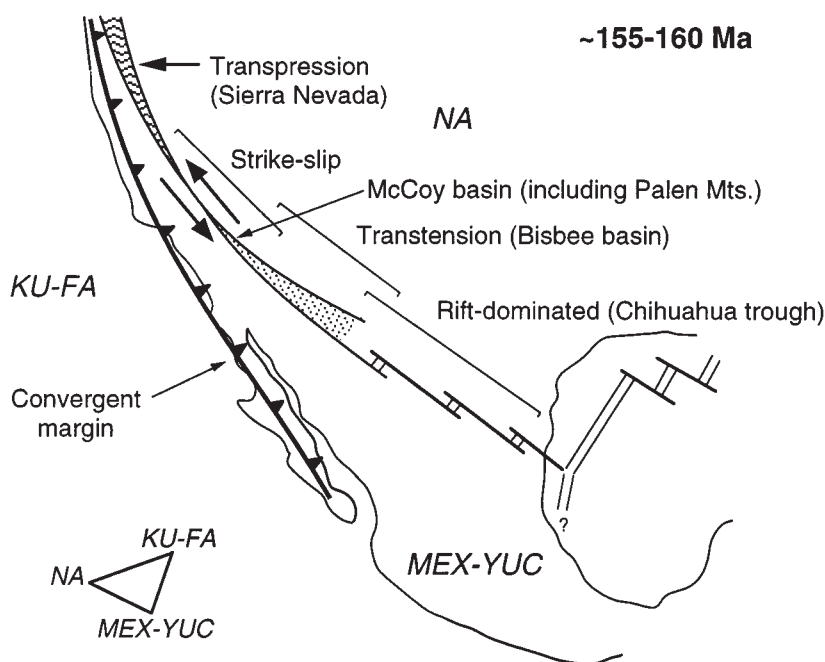


Figure 13. Hypothetical tectonic setting for the opening of the McCoy and Bisbee basins (modified from Dickinson et al., 1987, and Saleeby and Busby, 1992; plate motion vectors from May et al., 1989). Basin formation is attributed to exploitation of the thermally weakened welt of the arc by an aulocogen associated with the opening of the Gulf of Mexico (Bilodeau, 1982; Dickinson et al., 1987). The more abrupt volcanic to sedimentary transition in the McCoy basin, relative to the Bisbee basin, is attributed to a higher component of strike-slip there (Saleeby and Busby-Spera, 1992). This is a response to changing conditions along the curving boundary between North America (NA) and Mexico-Yucatan (MEX-YUC).

of the lower McCoy Mountains Formation in order to accumulate as much as 3 km of fluvial and lacustrine strata. Perhaps the Bisbee Group records relatively active rifting (*sensu* McKenzie, 1978) characterized by thermal doming, graben formation, and higher rates of volcanism. The lower McCoy Mountains Formation, in contrast, records more passive rifting (*sensu* Steckler and Brink, 1986), with a greater strike slip component (Adams et al., 1991; Saleeby and Busby-Spera, 1992). Because of the strong northward component of absolute motion of North America and the curvature of the plate margin, a greater component of strike-slip faulting relative to extension would be expected as one moves north along the plate margin from the Bisbee basin to the McCoy basin (Fig. 13).

ACKNOWLEDGMENTS

This research was supported by National Science Foundation grant EAR 90-18606 to Busby and Mattinson and grant EAR 92-19739 to Busby, and two University of California, Santa Barbara Geology Department Fellowships to Fackler-Adams. We thank Paul Stone for suggesting the problem to us, taking us on a reconnaissance trip to the area, assisting in zircon sampling,

returning to examine field relations, and providing an insightful review of an early draft of the manuscript. We also thank Kari Bassett for an informal review; Yemane Asmerom, Gordon Haxel, and Steve Reynolds for formal reviews of the manuscript; Nancy Riggs, William Morris, Cliff Hopson, Elizabeth Schermer, and James Sample for valuable discussions in the lab and in the field; and Charles Weiland for able field assistance.

REFERENCES CITED

- Adams, B. N., Busby-Spera, C. J., Stone, P., and Mattinson, J. M., 1991, New stratigraphic and chronologic controls on Jurassic magmatism and tectonics in the Mojave-Sonora desert: Evidence from the Palen Mountains (Southeastern Mojave): *Geological Society of America Abstracts with Programs*, v. 23, no. 5, p. A250.
- Anderson, J. L., 1983, Proterozoic anorogenic granite plutonism of North America, in Medaris, L. G., Byers, C. W., and Shanks, W. C., eds., *Proterozoic geology*: Geological Society of America Memoir 161, p. 133-154.
- Anderson, P., 1989, Proterozoic plate tectonic evolution of Arizona, in Jenny, J. P., and Reynolds, S. J., eds., *Geological Evolution of Arizona*: Arizona Geological Society Digest, v. 17, p. 17-55.
- Bassett, K. N., and Busby, C. J., 1996, Interstratified rhyolite dome and andesite volcanic deposits in the Late Jurassic (?) Temporal-Bathub Formations in southern Arizona: *Geological Society of America Abstracts with Programs*, v. 28, no. 7, p. A-114.
- Bilodeau, W. L., 1982, Tectonic models for Early Cretaceous rifting in southeastern Arizona: *Geology*, v. 10, p. 466-470.

- Bilodeau, W. L., and Keith, S. B., 1979, Intercalated volcanics and eolian "Aztec-Navajo-like" sandstones in Southeast Arizona; another clue to the Jurassic-Triassic paleotectonic puzzle of the Southwestern U.S.: *Geological Society of America Abstracts with Programs*, v. 11, p. 70.
- Bilodeau, W. L., and Keith, S. B., 1984, Early Jurassic eolian "Navajo-Aztec-like" sandstones in southeast Arizona and their paleogeographic significance: *Geological Society of America Abstracts with Programs*, v. 16, p. 215.
- Bilodeau, W. L., and Keith, S. B., 1986, Lower Jurassic Navajo-Aztec-equivalent sandstones in southern Arizona and their paleogeographic significance: *American Association of Petroleum Geologists Bulletin*, v. 70, p. 690-701.
- Blakey, R. C., Peterson, F., and Kocurek, G., 1988, Synthesis of late Paleozoic and Mesozoic eolian deposits on the western interior of the United States, in Kocurek, G., ed., *Late Paleozoic and Mesozoic eolian deposits on the western interior of the United States*: *Sedimentary Geology*, v. 56, p. 3-125.
- Burchfiel, B. C., and Davis, G. A., 1972, Structural framework and evolution of the southern part of the Cordilleran orogen, western United States: *American Journal of Science*, v. 272, p. 97-118.
- Busby-Spera, C. J., 1988, Speculative tectonic model for the early Mesozoic arc of the southwest Cordilleran United States: *Geology*, v. 16, p. 1121-1125.
- Busby-Spera, C. J., and Kokelaar, P., 1991, Controls of the Sawmill Canyon fault zone on Jurassic magmatism and extension-transension in southern Arizona: *Geological Society of America Abstracts with Programs*, v. 23, no. 5, p. A250.
- Busby-Spera, C. J., and Kokelaar, P., 1992, Development of calderas in a transtensional fault zone: *International Geological Congress, 29th, Abstracts, Kyoto, Japan*, v. 29, p. 482.
- Busby-Spera, C. J., Mattinson, J. M., and Riggs, N. R., 1987, Lower Mesozoic extensional continental arc, Arizona and California: A depocenter for craton-derived quartz arenites: *Geological Society of America Abstracts with Programs*, v. 19, p. 607.
- Busby-Spera, C. J., Mattinson, J. M., and Adams, B. N., 1989, The Jurassic transition from continental intraarc extension to Gulf of Mexico-related rifting in the southwest Cordillera: *Eos (Transactions, American Geophysical Union)*, v. 70, p. 1300.
- Busby-Spera, C. J., Mattinson, J. M., Riggs, N. R., and Schermer, E. R., 1990a, The Triassic-Jurassic magmatic arc in the Mojave-Sonora deserts and the Sierran-Klamath region: Similarities and differences in paleogeographic evolution, in Harwood, D., and Miller, M., eds., *Late Paleozoic and Mesozoic paleogeographic relations, Klamath-Sierra and adjacent regions*: *Geological Society of America Special Paper* 225, p. 325-337.
- Busby-Spera, C. J., Mattinson, J. M., and Schermer, E. R., 1990b, Stratigraphic and tectonic evolution of the Jurassic arc: New field and U-Pb zircon geochronological data from the Mojave Desert: *Geological Society of America Abstracts with Programs*, v. 22, no. 3, p. 11-12.
- Chan, M. A., and Kocurek, G., 1988, Complexities in eolian and marine interactions: Processes and eustatic controls on erg development, in Kocurek, G., ed., *Late Paleozoic and Mesozoic eolian deposits on the western interior of the United States*: *Sedimentary Geology*, v. 56, p. 283-300.
- Condie, K. C., 1982, Plate-tectonic model for Proterozoic continental accretion in the southwestern United States: *Geology*, v. 10, p. 37-42.
- Crowl, W. J., 1979, *Geology of the central Dome Rocks Mountains, Arizona* [M.S. thesis]: Tucson, University of Arizona, 76 p.
- Dickinson, W. R., and Suczek, C. A., 1979, Plate tectonics and sandstone compositions: *American Association of Petroleum Geologists Bulletin*, v. 63, p. 2164-2182.
- Dickinson, W. R., Harbaugh, D. W., Saller, A. H., Heller, P. L., and Snyder, W. S., 1983, Detrital modes of upper Paleozoic sandstones derived from the Antler orogeny in Nevada: Implications for the nature of the Antler orogeny: *American Journal of Science*, v. 283, p. 481-509.
- Dickinson, W. R., Fiorillo, A. R., Rogelio, D. H., Potochnik, A. R., and Swift, P. N., 1986, Cretaceous strata of southern Arizona, in Jenney, J. P., and Reynolds, S. J., eds., *Geological evolution of Arizona*: Arizona Geological Society Digest 17.
- Dickinson, W. R., Klute, M. A., and Swift, P. N., 1987, The Bisbee basin and its bearing on late Mesozoic paleo-

- geographic and paleotectonic relations between the Cordilleran and Caribbean regions, in Abbott, P., ed., Cretaceous stratigraphy, western North America: Los Angeles, California, Pacific Section, Society of Economic Paleontologists and Mineralogists, p. 51–62.
- Everett, B. H., Kowallis, B. J., and Christiansen, E. H., 1989, Correlation of Jurassic sediments of southern Utah using bentonite characteristics: Geological Society of America Abstracts with Programs, v. 21, no. 5, p. 77.
- Fisher, R. V., and Schminke, H. U., 1984, Pyroclastic rocks: New York, Springer-Verlag, 472 p.
- Fleck, R. J., Mattinson, J. M., Busby, C. J., Carr, M. D., Davis, G. A., and Burchfiel, B. C., 1994, Isotopic complexities and the age of the Delfonte volcanic rocks, eastern Mescal Range, southeastern California: Stratigraphic and tectonic implications: Geological Society of America Bulletin, v. 106, p. 1242–1253.
- Folk, R. L., 1972, Petrology of Sedimentary Rocks, University of Texas Geology: Austin, Texas, Hemphill's Bookstore, 170 p.
- Gradstein, F. M., Agterberg, F. P., Ogg, J. G., Hardenbol, J., van Veen, P., Theirry, J., and Huang, Z., 1994, A Mesozoic time scale: Journal of Geophysical Research, v. 99, p. 24051–24074.
- Hamilton, W. J., 1982, Structural evolution of the Big Maria Mountains, northeastern Riverside County, southeastern California, in Frost, E., and Martin, D. L., eds., Mesozoic-Cenozoic tectonic evolution of the Colorado River region, California, Arizona, and Nevada: San Diego, California, Cordilleran Publishers, p. 1–28.
- Hamilton, W. J., 1987, Mesozoic geology and tectonics of the Big Maria Mountains region, southeastern California, in Dickinson, W. R., and Klute, M. A., eds., Mesozoic rocks of southern Arizona and adjacent areas: Arizona Geological Society Digest, v. 18, p. 33–47.
- Harding, L. E., 1982, Tectonic significance of the McCoy Mountains Formation, southeastern California and southwestern Arizona [Ph.D. dissert.]: Tucson, University of Arizona, 197 p.
- Harding, L. E., and Coney, P. J., 1985, The geology of the McCoy Mountains Formation, southeastern California and southwestern Arizona: Geological Society of America Bulletin, v. 96, p. 755–769.
- Harding, L. E., Butler, R. F., and Coney, P. J., 1980, Paleomagnetic evidence for a Jurassic age assignment on a 6 km thick sedimentary terrane in southwestern Arizona and southeastern California: Geological Society of America Abstracts with Programs, v. 12, p. 109.
- Harding, L. E., Butler, R. F., and Coney, P. J., 1983, Paleomagnetic evidence for Jurassic deformation of the McCoy Mountains Formation, southeastern California and southwestern Arizona: Earth and Planetary Science Letters, v. 62, p. 104–144.
- Howard, K. A., and John, B. E., 1987, Crustal extension along a rooted system of imbricate low-angle faults: Colorado River extensional corridor, California and Arizona, in Coward, M. P., Dewey, J. F., and Hancock, P. L., eds., Continental extensional tectonics: Geological Society [London] Special Publication 28, p. 299–311.
- LeVeque, R. A., 1982, Stratigraphy and structure of the Palen formation, Palen Mountains, southeastern California, in Frost, E. G., and Martin, D. L., eds., Mesozoic-Cenozoic tectonic evolution of the Colorado River region, California, Arizona, and Nevada: San Diego, California, Cordilleran Publishers, p. 267–273.
- Lipman, P. W., and Hagstrum, J. T., 1992, Jurassic ash-flow sheets, calderas, and related intrusions of the Cordilleran volcanic arc in southeastern Arizona: Implications for regional tectonics and ore deposits: Geological Society of America Bulletin, v. 104, p. 32–39.
- Ludwig, K. R., 1991, ISOPLOT: A plotting and regression program for radiogenic-isotope data (version 2.57), U.S. Geological Survey Open-File report 91–445 (revised 1992), 40 p.
- Marzolf, J. E., 1980, The Aztec Sandstone and stratigraphically related rocks in the Mojave desert, in Fife, D. L., and Brown, G. R., eds., Geology and mineral wealth of the California desert: Santa Ana, California, South Coast Geological Society, p. 215–220.
- Mattinson, J. M., 1984, Labile Pb in young, high-U zircons: Geological Society of America Abstracts with Programs, v. 16, p. 586.
- Mattinson, J. M., 1987, U-Pb ages of zircons; a basic examination of error propagation: Chemical Geology, v. 66, p. 151–162.
- Mattinson, J. M., 1994, A study of complex discordance in zircons using step-wise dissolution techniques: Contributions to Mineralogy and Petrology, v. 116, p. 117–129.
- May, S. R., 1985, Paleomagnetism of Jurassic volcanic rocks in southeastern Arizona and North American Jurassic apparent polar wander [Ph.D. dissert.]: Tucson, University of Arizona, 227 p.
- May, S. R., Beck, M. E., Jr., and Butler, R. F., 1989, North American apparent polar wander, plate motion, and left-oblique convergence, Late Jurassic–Early Cretaceous orogenic consequences: Tectonics, v. 8, p. 433–451.
- McKenzie, D. P., 1978, Some remarks on the development of sedimentary basins: Earth and Planetary Science Letters, v. 40, p. 25–32.
- Mellors, R. A., Waitt, R. B., and Swanson, D. A., 1988, Generation of pyroclastic flows and surges by hot-rock avalanches from the dome of Mount St. Helens volcano, USA: Bulletin of Volcanology, v. 50, p. 14–25.
- Miller, E. L., and Busby, C. J., 1995, eds., Jurassic magmatism and tectonics of the North American Cordillera: Geological Society of America Special Paper 299, 425 p.
- Miller, E. L., and Carr, M. D., 1978, Recognition of possible Aztec-equivalent sandstones and associated Mesozoic metasedimentary deposits within the Mesozoic magmatic arc in the southwestern Mojave Desert, in Howell, D. G., and McDougall K. A., eds., Mesozoic Paleogeography of the western United States: Pacific Section, Society of Economic Paleontologists and Mineralogists, Pacific Coast Paleogeography Symposium 2, p. 283–289.
- Nakada, S., and Fujii, T., 1993, Preliminary report on the activity at Unzen volcano (Japan), November 1990–November 1991: Dacite lava domes and pyroclastic flows: Journal of Volcanology and Geothermal Research, v. 54, p. 319–333.
- Nelson, B. K., and dePaolo, D. J., 1985, Rapid production of continental crust 1.7 to 1.9 by ago: Nd isotopic evidence from the basement of the North American midcontinent: Geological Society of America Bulletin, v. 96, p. 746–754.
- Pelka, G. J., 1973, Geology of the McCoy and Palen Mountains, southeastern California [Ph.D. dissert.]: Santa Barbara, University of California, 162 p.
- Pindell, J. L., 1985, Alleghanian reconstruction and subsequent evolution of the Gulf of Mexico, Bahamas, and Proto-Caribbean: Tectonics, v. 4, p. 1–39.
- Reynolds, S. J., Spencer, J. E., and DeWitt, E., 1987, Stratigraphic and U-Th-Pb geochronology of Triassic and Jurassic rocks in west-central Arizona, in Dickinson, W. R., and Klute, M. A., eds., Mesozoic geology of southern Arizona and adjacent areas: Arizona Geological Society Digest, v. 18, p. 65–80.
- Reynolds, S. J., Spencer, J. E., Asmeron, Y., DeWitt, E., and Laubach, S. E., 1989, Early Mesozoic uplift in west-central Arizona and southeastern California: Geology, v. 17, p. 207–211.
- Richard, S. M., Reynolds, S. J., and Spencer, J. E., 1985, Mesozoic thrust sheets of the Harquahala and Little Harquahala Mountains, western Arizona: Geological Society of America Abstracts with Programs, v. 17, p. 404.
- Riggs, N. R., Mattinson, J. M., and Busby-Spera, C., 1986, U-Pb ages of the Mount Wrightson Formation, south-central Arizona, and possible correlation with the Navajo sandstone: Eos (Transactions, American Geophysical Union), v. 67, p. 1249.
- Riggs, N. R., Mattinson, J. M., and Busby, C. J., 1993, Correlation of Jurassic eolian strata between the magmatic arc and the Colorado Plateau: New U-Pb geochronologic data from southern Arizona: Geological Society of America Bulletin, v. 105, p. 1231–1246.
- Rodríguez-Elizarrarás, S., Siebe, C., Komorowski, J.-C., Espíndola, J. M., and Saucedo, R., 1991, Field observations of pristine block-and-ash flow deposits emplaced April 16–17, 1991 at Volcán de Colima, Mexico: Journal of Volcanology and Geothermal Research, v. 48, p. 399–412.
- Saleeby, J., and Busby-Spera, C. J., 1992, Early Mesozoic tectonic evolution of the western U.S. Cordillera, in Burchfiel, B. C., Lipman, P. W., and Zoback, M. L., eds., The Cordilleran Orogen: Conterminous U.S.: Boulder, Colorado, Geological Society of America, The geology of North America, v. G-3, p. 107–168.
- Schmid, R., 1981, Descriptive nomenclature and classification of pyroclastic deposits and fragments: Recommendations of the IUGS Subcommittee on the Systematics of Igneous Rocks: Geology, v. 9, p. 41–43.
- Silver, L. T., and Anderson, T. H., 1974, Possible left-lateral early to middle Mesozoic disruption of the southwestern North American craton margin: Geological Society of America Abstracts with Programs, v. 6, no. 7, p. 955–956.
- Sparks, R. J. S., Self, S., and Walker, G. P. L., 1973, Products of ignimbrite eruptions: Geology, v. 1, p. 115–118.
- Spencer, J. E., and Reynolds, S. J., 1989, Middle Tertiary tectonics of Arizona and adjacent areas, in Jenny, J. P., and Reynolds, S. J., eds., Geological evolution of Arizona: Arizona Geological Society Digest, v. 17, p. 539–574.
- Steckler, M. S., and Brink, U. S., 1986, Lithospheric strength variations as a control on new plate boundaries: Examples from the northern Red Sea region: Earth and Planetary Science Letters, v. 79, p. 120–132.
- Stone, P., and Kelly, M. M., 1988, Preliminary geologic map of the Palen Pass quadrangle, Riverside County, California: U.S. Geological Survey Open-File Report 88–503, scale 1:24 000.
- Stone, P., and Pelka, G. J., 1989, Geologic map of the Palen-McCoy Wilderness Study area and vicinity, Riverside County, California: U.S. Geological Survey Map MF-2090, scale 1:62 500.
- Stone, P., and Stevens, C. H., 1988, Pennsylvanian and Early Permian paleogeography of east-central California: Implications for the shape of the continental margin and the timing of continental truncation: Geology, v. 16, p. 330–333.
- Stone, P., Page, V. M., Hamilton, W., and Howard, K. A., 1987, Cretaceous age of the upper part of the McCoy Mountains Formation, southeastern California and southwestern Arizona, and its tectonic significance: Reconciliation of paleobotanical and paleomagnetic evidence: Geology, v. 15, p. 561–564.
- Tosdal, R. M., 1986, Mesozoic ductile deformation in the southern Dome Rock Mountains, northern Trigo Mountains, Trigo Peaks, and Livingston Hills, southwestern Arizona, and Mule Mountains, southeastern California, in Beatty, B., and Stone, C., eds., Frontiers in geology and ore deposits of Arizona and the southwest: Arizona Geological Society Digest, v. 16, p. 62–71.
- Tosdal, R. M., and Stone, P., 1994, Stratigraphic relations and U-Pb geochronology of the Upper Cretaceous upper McCoy Mountains Formation, southwestern Arizona: Geological Society of America Bulletin, v. 106, p. 476–491.
- Tosdal, R. M., Haxel, G. B., and Wright, J. E., 1989, Jurassic geology of the Sonoran Desert region, southern Arizona, southeastern California, northernmost Sonora: Construction of a continental-margin magmatic arc, in Jenny, J. P., and Reynolds, S. J., eds., Geological evolution of Arizona: Arizona Geological Society Digest, v. 17, p. 397–434.
- Walker, J. D., 1988, Permian and Triassic rocks of the Mojave Desert and their implications for timing and mechanism of continental truncation: Tectonics, v. 7, p. 685–709.
- Wright, J. E., Haxel, G., and May, D. J., 1981, Early Jurassic uranium-lead isotopic ages for Mesozoic supracrustal sequences, Papago Indian Reservation, southern Arizona: Geological Society of America Abstracts with Programs, v. 13, p. 115.
- Yamamoto, T., Takarada, S., and Suto, S., 1993, Pyroclastic flows from the 1991 eruption of Unzen volcano, Japan: Bulletin of Volcanology, v. 55, p. 166–175.

MANUSCRIPT RECEIVED BY THE SOCIETY JUNE 27, 1996
 REVISED MANUSCRIPT RECEIVED FEBRUARY 4, 1997
 MANUSCRIPT ACCEPTED APRIL 16, 1997